

Assessing the Climate Impacts of the Observed Atlantic Multidecadal Variability Using the GFDL CM2.1 and NCAR CESM1 Global Coupled Models

YOHAN RUPRICH-ROBERT

Atmosphere and Ocean Sciences, Princeton University, and NOAA/Geophysical Fluid Dynamics Laboratory, Princeton, New Jersey

RYM MSADEK

NOAA/Geophysical Fluid Dynamics Laboratory, Princeton, New Jersey, and CECI UMR 5318, CNRS/CERFACS, Toulouse, France

FREDERIC CASTRUCCIO AND STEPHEN YEAGER

Climate and Global Dynamics Laboratory, National Center for Atmospheric Research,^a Boulder, Colorado

TOM DELWORTH

NOAA/Geophysical Fluid Dynamics Laboratory, Princeton, New Jersey

GOKHAN DANABASOGLU

Climate and Global Dynamics Laboratory, National Center for Atmospheric Research,^a Boulder, Colorado

(Manuscript received 11 February 2016, in final form 8 November 2016)

ABSTRACT

The climate impacts of the observed Atlantic multidecadal variability (AMV) are investigated using the GFDL CM2.1 and the NCAR CESM1 coupled climate models. The model North Atlantic sea surface temperatures are restored to fixed anomalies corresponding to an estimate of the internally driven component of the observed AMV. Both models show that during boreal summer the AMV alters the Walker circulation and generates precipitation anomalies over the whole tropical belt. A warm phase of the AMV yields reduced precipitation over the western United States, drier conditions over the Mediterranean basin, and wetter conditions over northern Europe. During boreal winter, the AMV modulates by a factor of about 2 the frequency of occurrence of El Niño and La Niña events. This response is associated with anomalies over the Pacific that project onto the interdecadal Pacific oscillation pattern (i.e., Pacific decadal oscillation–like anomalies in the Northern Hemisphere and a symmetrical pattern in the Southern Hemisphere). This winter response is a lagged adjustment of the Pacific Ocean to the AMV forcing in summer. Most of the simulated global-scale impacts are driven by the tropical part of the AMV, except for the winter North Atlantic Oscillation–like response over the North Atlantic–European region, which is driven by both the subpolar and tropical parts of the AMV. The teleconnections between the Pacific and Atlantic basins alter the direct North Atlantic local response to the AMV, which highlights the importance of using a global coupled framework to investigate the climate impacts of the AMV. The similarity of the two model responses gives confidence that impacts described in this paper are robust.

Supplemental information related to this paper is available at the Journals Online website: <http://dx.doi.org/10.1175/JCLI-D-16-0127.s1>.

^aThe National Center for Atmospheric Research is sponsored by the National Science Foundation.

Corresponding author e-mail: Yohan Ruprich-Robert, yohan.ruprich-robert@noaa.gov

1. Introduction

During the last century, the observed annual mean North Atlantic sea surface temperatures (SSTs) have exhibited a long-term warming trend superimposed onto multidecadal fluctuations. This multidecadal variability has been referred to as the Atlantic multidecadal oscillation (AMO) by Kerr (2000). In the present study,

we use the term Atlantic multidecadal variability (AMV) rather than AMO, as there is so far no firm evidence of a unique periodicity in the multidecadal fluctuations of the North Atlantic SST (e.g., Gray et al. 2004; Knudsen et al. 2011; Frankcombe et al. 2010). The SST anomalies that define the AMV are characterized by a basin-scale anomalous pattern that has the same sign over the whole North Atlantic, as was first described by Kushnir (1994) and Schlesinger and Ramankutty (1994). These SST anomalies are uniform in sign but show a maximum loading over the subpolar gyre (SPG) region extending to the subtropics through the eastern side of the basin [see Knight et al. (2005), Trenberth and Shea (2006), and Ting et al. (2009, 2014) for different estimates of the AMV time series and spatial structure].

The origins of the observed AMV are still uncertain. Numerous studies based on global climate model (GCM) simulations have shown that the northward oceanic heat transport fluctuations associated with the Atlantic meridional overturning circulation (AMOC) variability are the main driver of the AMV (e.g., Knight et al. 2005; Zhang 2008; Medhaug and Furevik 2011; Ruprich-Robert and Cassou 2015). Yet, during the last century, the North Atlantic SST has also been affected by changes in external forcing, both anthropogenic (Chang et al. 2011; Booth et al. 2012) and natural (Otterå et al. 2010; Swingedouw et al. 2013), making the assessment of the contribution of the internal AMOC fluctuations to the observed AMV difficult (e.g., Rotstayn and Lohmann 2002; Terray 2012).

Whatever its origins, there is observational evidence that the AMV is associated with, and possibly the source of, marked climate anomalies over many areas of the globe. Sutton and Hodson (2005) and Sutton and Dong (2012) argued for the existence of a causal link between the warm phase of the AMV (referred to as the positive phase; AMV+) and warmer conditions over central Europe, drier conditions over the Mediterranean basin, and wetter conditions over northern Europe during boreal summer. Other studies have linked AMV+ to a warmer and drier climate over North America (Enfield et al. 2001; Sutton and Hodson 2007; Schubert et al. 2009; Kushnir et al. 2010). Consistent with these North American and European climate impacts, a number of studies suggested that the AMV could impact the mid-latitude winter atmospheric circulation by modulating the number of blocking events over the North Atlantic–Europe (NAE) region (Häkkinen et al. 2011; Davini et al. 2015) or by driving North Atlantic Oscillation (NAO)-like anomalies (Peings and Magnusdottir 2014, 2015; Omrani et al. 2014; Gastineau and Frankignoul 2015). McCabe et al. (2004) and more recently Chylek

et al. (2014) further linked the multidecadal North American drought frequency with both the AMV and its Pacific counterpart, the interdecadal Pacific oscillation [IPO; e.g., Zhang et al. 1997; Power et al. 1999; see Newman et al. (2016) for a recent review of the Pacific decadal variability]. Yet, whether these concomitant forcings of the Atlantic and Pacific arise from a coincidence or reveal a causal link between Atlantic and Pacific decadal anomalies remains uncertain.

In addition to impacting the Northern Hemisphere midlatitudes, the AMV has been shown to have significant impact on tropical climate with a decrease of South American rainfall and an intensification of West African and East Asian monsoons observed and simulated during AMV+ (e.g., Folland et al. 2001; Zhang and Delworth 2006; Mohino et al. 2011; Wang et al. 2012; Martin and Thorncroft 2014; Krishnamurthy and Krishnamurthy 2015). Vimont and Kossin (2007), following Goldenberg et al. (2001), have further shown that the AMV can impact Atlantic hurricane activity, with more hurricanes occurring during AMV+.

The numerous AMV teleconnections listed above highlight the importance of better understanding and predicting the AMV. However, the shortness of the historical record compared to the AMV period suggested by observations (~60–80 yr; cf. Fig. 1a) makes it difficult to rigorously isolate the drivers and the impacts of the AMV. In this context, numerical coupled climate models offer a valuable alternative to investigate AMV impacts and associated mechanisms. Ting et al. (2011, 2014) showed that the historical simulations from phase 3 of the Coupled Model Intercomparison Project (CMIP3) were able to reproduce some of the observed climate impacts associated with the AMV, like rainfall over Sahel and the Amazon, but they stressed the lack of any statistically significant response in terms of precipitation over the United States and Southeast Asia.

However, estimating the impacts of the AMV using GCM can only offer limited insight into the observed teleconnections insofar as the simulated AMV pattern is usually different from the observed one (e.g., Zhang and Wang 2013). To tackle this issue, Zhang and Delworth (2006) used a hybrid coupled model in which the fully dynamic ocean component was replaced by a horizontally motionless slab ocean over the Atlantic constrained through heat flux corrections to follow the twentieth-century evolution of the observed AMV. They showed that the observed AMV yields climate impacts in the North Pacific that project onto the northern part of the IPO. They argued that this forcing occurs through changes in the Northern Hemisphere storm tracks and through a reinforcement of the response by ocean dynamics and positive air–sea feedbacks over the North

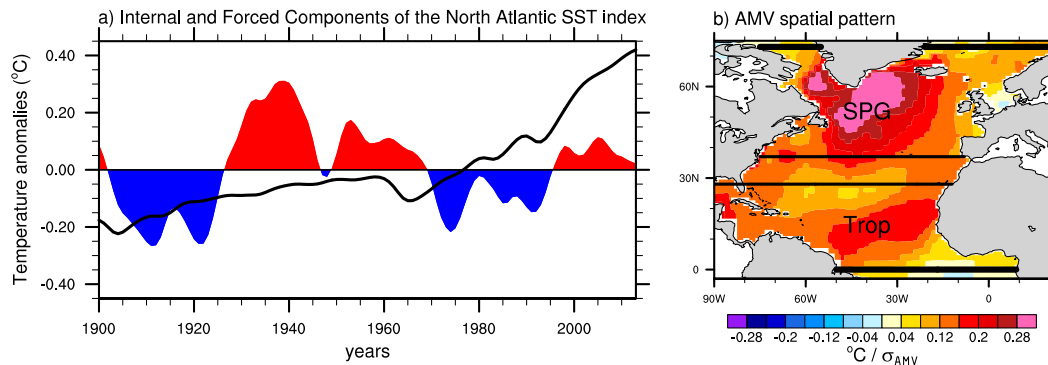


FIG. 1. (a) Internal (red and blue) vs external (black line) components of the observed North Atlantic SST decadal variability following the Ting et al. (2009) definition. (b) Regression map of the observed annual mean SST (ERSST.v3; Smith et al. 2008) on the internal component of the North Atlantic SST index (i.e., the AMV index; units are degrees Celsius per std dev of AMV index). Both SST field and AMV index time series have been low-pass filtered prior to computing the regression, using a Lanczos filter (21 weights with a 10-yr cutoff period). The black latitude lines in (b) show the subpolar and tropical domains used for the SPG_AMV and Trop_AMV experiments (see section 2b).

Pacific (Zhang and Delworth 2007). Their proposed mechanism hence involved mainly an extratropical teleconnection. This contrasts with Dong et al. (2006), who used a different approach in which the coupled model SSTs were relaxed toward fixed SST anomalies corresponding to the observed AMV to argue that the link occurred through a tropical Atlantic–tropical Pacific teleconnection that involved changes in the Walker circulation (WC). Neither of these studies investigated the respective role played by the extratropical and the tropical parts of the AMV. Recent studies focused on the impact of the tropical Atlantic on the tropical Pacific at decadal time scales corroborated Dong et al. (2006)’s mechanism (Kucharski et al. 2011, 2015; McGregor et al. 2014; Li et al. 2015; Ham and Kug 2015; Zanchettin et al. 2016). However, the mechanism proposed by Zhang and Delworth (2007) could still hold in addition to the tropical teleconnection, and the relative importance of each teleconnection in setting the Pacific response to the AMV remains to be established.

Given the numerous potential climate impacts of the AMV at decadal time scale, it is crucial to improve our knowledge of the mechanisms associated with AMV teleconnections. A better understanding of these mechanisms could help advance the prediction of AMV impacts. In this study, we investigate the global impacts of the observed AMV, identify the respective role played by the extratropical and tropical parts of the AMV, and estimate the importance of the other oceanic basins in modulating the global AMV impacts. We use a model approach similar to Dong et al. (2006), but using two different GCMs and large-ensemble simulations for both models. The structure of the paper is as follows. The model setup and the idealized experiments are

described in section 2. The simulated AMV climate impacts are documented in section 3, and their mechanisms are investigated in Section 4. Section 5 focuses on the tropical Pacific response to the AMV. We assess the signal-to-noise ratio of the response to the AMV in section 6 before concluding and discussing the results in sections 7 and 8.

2. Methodology

We perform idealized experiments using two global coupled models in which the North Atlantic SSTs are restored to a time-independent spatial pattern corresponding to an estimate of the internally driven component of the observed AMV anomaly.

a. Decomposing the internal and forced components of the observed AMV

To isolate the internal component of the observed AMV from the externally forced part, we follow the approach proposed by Ting et al. (2009). In this method the externally forced SST variability is estimated by applying a signal-to-noise maximizing EOF analysis to the global annual mean SST derived from the CMIP5 multimodel ensemble (only one simulation from each of the 36 models has been used to reduce the bias toward any specific model). Historical simulations and representative concentration pathway 8.5 (RCP8.5) simulations are chosen for the 1870–2005 and the 2006–13 periods, respectively. The time series associated with the leading global signal-to-noise EOF [i.e., the first principal component (PC1)] is taken as the time series of the radiatively forced component of SST. The spatial pattern of the forced component of the observed

SST is obtained by regressing the observed global SST onto the PC1 time series. The observed SST dataset is from the Extended Reconstructed Sea Surface Temperature, version 3 (ERSST.v3; Smith et al. 2008). The internal component of the observed North Atlantic SST index (hereafter referred to as the AMV index for clarity) is then obtained as the residual of the observed North Atlantic basinwide average SST (from the equator to 60°N and from 75° to 7.5°W) after subtracting the forced component (Fig. 1a). The spatial pattern of the AMV is obtained by regressing the annual mean observed SST at each grid point onto the AMV index (Fig. 1b). Both the AMV time series and the SST field have been low-pass filtered prior to the regression using a Lanczos filter (21 weights with a 10-yr cutoff period), and the regression has been computed over the 1870–2013 period.

b. Description of the coupled model experiments

We use two different coupled models in this study: the GFDL CM2.1 and the NCAR CESM1(CAM5) (hereafter CESM1). The detailed formulation and simulation characteristics of CM2.1 are described by Delworth et al. (2006) and Wittenberg et al. (2006). The ocean component of CM2.1 has 50 vertical levels and a 1° × 1° horizontal resolution, increasing to 1/3° meridional spacing near the equator. Its atmospheric component consists of 24 vertical levels and 2° latitude × 2.5° longitude grid spacing. CESM1 is used with the same components as the long control simulation of the CESM Large Ensemble Project (Kay et al. 2015). All components of CESM1 have approximately 1° horizontal resolution. The atmospheric component CAM5.2 has 30 hybrid vertical levels. The ocean component uses 60 vertical levels and a meridional mesh refinement down to 0.27° near the equator.

Five sets of experiments are performed:

- 1) Full_AMV+ and Full_AMV–: SST anomalies corresponding to plus or minus one standard deviation of the AMV index (i.e., plus or minus the AMV pattern shown in Fig. 1b) are imposed over the North Atlantic. In these experiments, the model daily SST is restored to the observed AMV anomalies superimposed on the model's own daily climatology over the North Atlantic region from 0° to 73°N. To prevent instabilities between the restored and un-restored regions, 8° buffer zones are defined over the northern and southern boundaries with a restoring coefficient decreasing by 0.125 per degree of latitude so that a full restoring is performed only between 8° and 65°N. Outside of the restoring region, the model evolves freely, allowing a full response of the climate system. Details on the restoring method are provided in the appendix.
- 2) Trop_AMV: Similar to the Full_AMV+ and Full_AMV– experiments but only the tropical part of the AMV is imposed from 0° to 28°N, with full restoring done between 8° and 20°N (see region in Fig. 1b).
- 3) SPG_AMV: Similar to the Full_AMV experiments but only the subpolar part of the AMV is imposed from 37° to 73°N, with full restoring done between 45° and 65°N (cf. Fig. 1b).
- 4) XTrop_AMV: Similar to the Full_AMV experiments but only the extratropical part of the AMV is imposed from 28° to 73°N, with full restoring done between 36° and 65°N. Because of computational constraints, these experiments have been done only with CM2.1.
- 5) Damped_Global_AMV: Similar to the Full_AMV experiments but in addition to restoring the North Atlantic to the observed AMV anomaly, the SST over each grid point of the globe outside of the North Atlantic is restored to its own climatology. These experiments have been done only with CM2.1.
- 6) Damped_TropPac_AMV: Similar to the Full_AMV experiments but in addition to the AMV being restored over the North Atlantic, the SSTs over the tropical Pacific (28°S–28°N from the Maritime Continent to the eastern Pacific border) are restored to their own climatology (see region in Fig. 9e). These experiments have been done only with CM2.1.

For all experiments we perform large-ensemble simulations with 100 members for CM2.1 and 30 members for CESM1 to robustly estimate the AMV climate impacts and their associated signal-to-noise ratio. As discussed later, the smaller ensemble size for CESM1 does not affect the robustness of the results. For CM2.1 the ocean and atmosphere of the ensemble members have been initialized randomly (5 years apart from each other) from an independent control integration. For CESM1, ensemble members are obtained using a combination of macro- (sampling three different ocean initial states) and micro- (perturbation of atmospheric initial conditions) ensemble generation, following Hawkins et al. (2015). To capture the potential response and adjustment of other oceanic basins to the AMV anomalies, the simulations have been integrated for 10 years. We chose not to extend the simulations beyond 10 years because of the presence of drift (see the online supplemental material). All external forcings are kept constant at their preindustrial values during the integrations.

Comparing the Full_AMV experiments to the Trop_AMV and SPG_AMV experiments allows us to attribute the climate impacts to particular subdomains of the

AMV pattern. Note that the anomalies imposed over a given region can propagate outside of the restoring region through atmospheric and oceanic teleconnections. Therefore, we chose to keep a 10° latitude band with no restoring between the tropical and extratropical subdomains in order to better separate the respective impacts of those parts of the AMV. The XTrop_AMV experiments will allow us to investigate the sensitivity of the climate response to the choice of the extratropical domain. For the Damped_Global_AMV case, the 5-day restoring of the model SST toward its climatology outside of the North Atlantic drastically inhibits the generation of SST anomalies in those regions through oceanic and low-frequency ocean–atmosphere feedback processes. These experiments provide information about the role played by ocean dynamical adjustment outside of the North Atlantic on the global AMV impacts simulated in the Full_AMV experiments. The Damped_TropPac_AMV experiments allow us to isolate the role played by the tropical Pacific response and, in particular, the El Niño–Southern Oscillation (ENSO) response in the AMV climate impacts.

Unless otherwise stated, the results presented in the article correspond to the ensemble mean of each experiment. Each year of the individual ensemble members is used to evaluate the statistical significance of the results using a two-sided Student's *t* test.

3. Results: Description of the global AMV climate impacts

a. The boreal summer response (June–September)

Restoring the two models to the observed AMV pattern yields as expected a temperature response very similar to observations over the North Atlantic, with the strongest warming over the Atlantic SPG ($\sim +0.5^\circ\text{C}$), extending in a comma-shaped pattern to the tropics ($\sim +0.3^\circ\text{C}$) (Figs. 2a,b). The magnitude of the simulated temperature anomalies is, however, not twice as high as the observed anomalies shown on Fig. 1b, as one would expect from the difference between a positive and a negative phase of the AMV. This is due to the fact that we do not impose a very strong nudging in the experimental protocol to allow ocean–atmosphere coupling and variability at high frequencies, which tend to dissipate the heat anomalies imposed at the surface.

The models simulate remarkably similar global teleconnections. We note a warming of about 0.1° – 0.15°C over the northern and eastern Indian Ocean and over the Maritime Continent. Over the Pacific, temperature anomalies project strongly onto a negative phase of the IPO (Fig. 3) with negative SST anomalies in the tropical

Pacific that extend toward the pole in both hemispheres in a horseshoe-like pattern that surrounds positive SST anomalies in the west. Unlike CESM1, CM2.1 simulates a warming over the central equatorial Pacific that breaks the spatial coherence of the IPO pattern. We will discuss in section 5 the possible reasons for this difference. Significant temperature anomalies are found over land, with positive anomalies larger than 0.3°C over the western part of the United States and over the Mediterranean region. In both models, a warming is also simulated over most of the Eurasian continent. The models show less agreement over the Southern Hemisphere, although both show a warming over northeastern Australia, over sub-Saharan Africa, and over South America. Finally, both models simulate a warming of the whole Arctic; however, the amplitude of this signal is much stronger in CESM1 than in CM2.1. Further analyses are ongoing to understand the reasons for the differences over this region.

The AMV warming leads to low pressure anomalies over most of the Northern Hemisphere, particularly over North America, the North Atlantic, and North Africa, with large anomalies over the subtropics in both models (Figs. 2c,d). The broad North Atlantic low pressure anomaly is mass compensated by positive pressure anomalies over most of the Pacific. Such a seesaw pattern indicates a modification of the WC by the AMV. This is consistent with the studies of McGregor et al. (2014) and Li et al. (2015), who suggest that over the last 30 years the tropical Atlantic warming has contributed to the strengthening of the WC, which is in contrast with the long-term weakening trend of the WC observed over the last century (Kociuba and Power 2015).

In addition to the SLP anomalies associated with the modification of the WC, there is a northward shift and a reinforcement of the northern part of the intertropical convergence zone (ITCZ) over the North Atlantic, the eastern Pacific, and the Sahel (Figs. 2e,f). Increased rainfall is also found over the equatorial Indian Ocean, whereas reduced precipitation prevails over the western and central tropical Pacific in both hemispheres. This corresponds to a southwestward tilt of the South Pacific convergence zone (SPCZ) and a southward shift of the ITCZ.

Over the extratropics, the two models simulate a small but significant rainfall increase over the North Atlantic that is consistent with the imposed SST warming, which increases the evaporation and thus the amount of precipitable water (not shown). Reduced rainfall is found over the extratropical eastern North Pacific especially in CM2.1, which is driven by both a decrease of atmospheric humidity convergence and a decrease of evaporation resulting from the simulated cold SST response (not shown). Both models tend to indicate a north–south

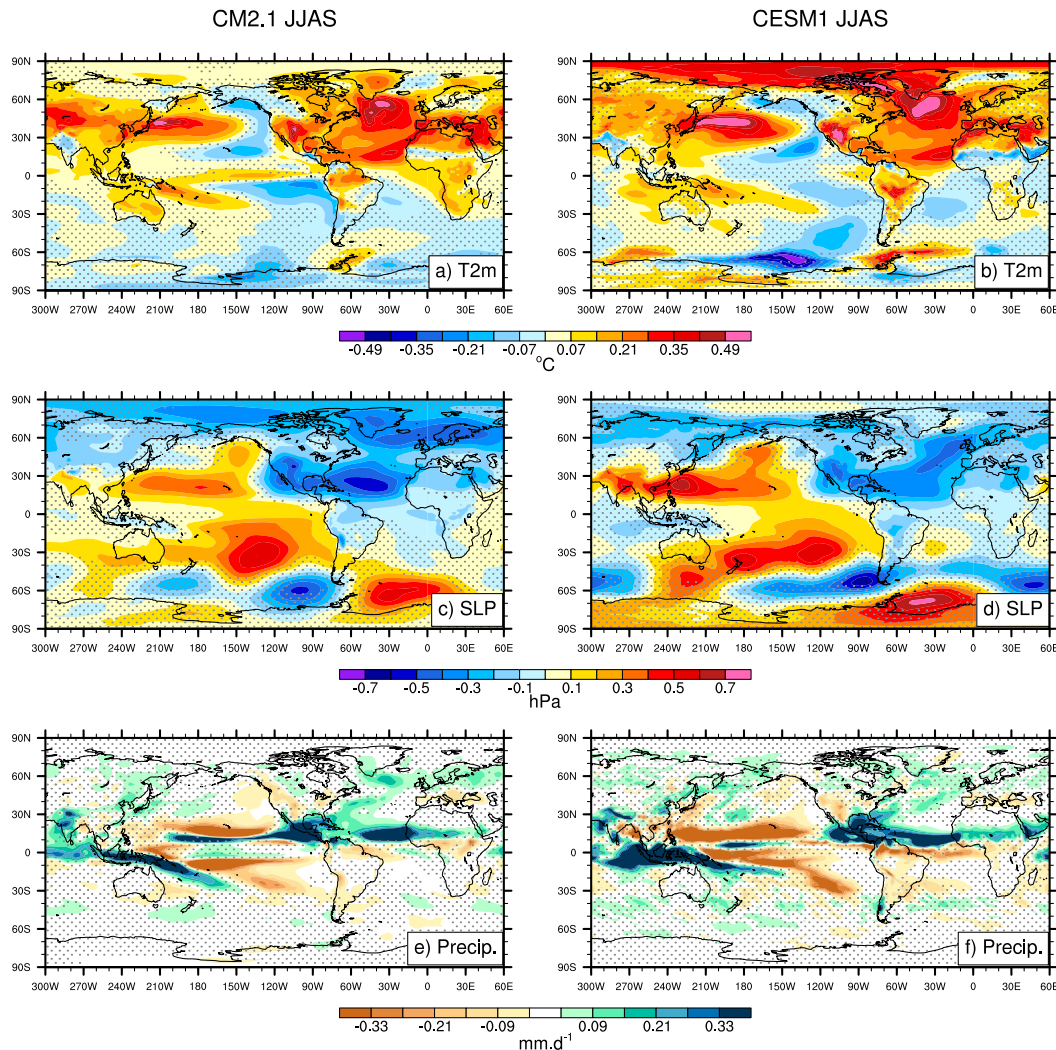


FIG. 2. Differences between the 10-yr average of the Full_AMV+ and the Full_AMV- ensemble simulations for the JJAS season. (a),(b) T2m, (c),(d) SLP, and (e),(f) precipitation. Results from (left) CM2.1 and (right) CESM1 are shown. Stippling indicates regions that are below the 95% confidence level of statistical significance according to a two-sided Student's t test. Note that the contours intervals of T2m in (a) and (b) have been multiplied by 1.75 compared to Fig. 1b to allow a straightforward comparison.

dipole of precipitation over Europe, with drier conditions over the Mediterranean area and wetter conditions over northern Europe (significant only in CM2.1), which is consistent with the documented impact of a positive AMV in observations (Sutton and Dong 2012). In agreement with Sutton and Hodson (2005) and Schubert et al. (2009), we also find that AMV+ is associated with warmer and drier conditions over the western part of the United States. The two models also show drier conditions over South America and precipitation increase over India, which suggests an impact of the AMV on the Asian monsoon, in agreement with previous observational studies (e.g., Seager et al. 2010a; Krishnamurthy and Krishnamurthy 2015).

b. The boreal winter response (December–March)

During December–March (DJFM), the simulated North Atlantic SSTs are less reminiscent of the imposed AMV pattern than during June–September (JJAS) especially over the SPG and in CM2.1 (Figs. 4a,b). This comes from the fact that, during winter, SSTs are less constrained by the restoring term because of the deeper mixed layer that dilutes the imposed anomaly over a deeper oceanic column. The pattern differences between the two models over the SPG come from a mixed layer deeper in CM2.1 than in CESM1 as well as from the presence of a drift mentioned in section 2b and detailed in the supplementary material (see Figs. S1–S3).

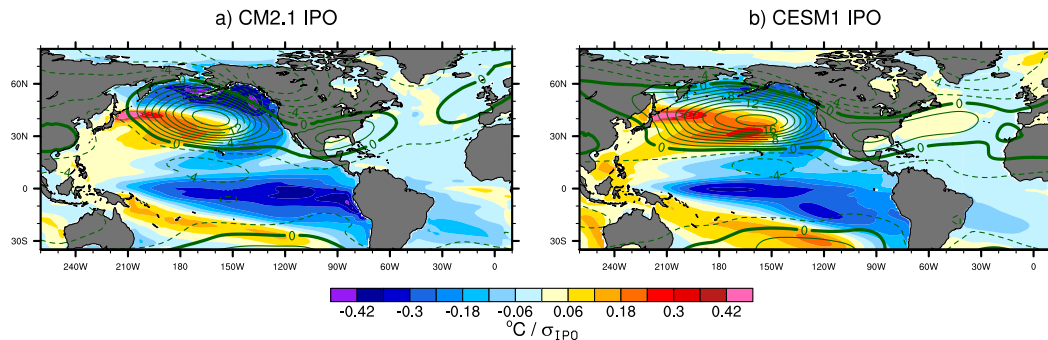


FIG. 3. Spatial structure of the IPO in (a) CM2.1 and (b) CESM1 as estimated by the regression of the annual mean SST (color shading; units are degrees Celsius per std dev of the IPO index) on the IPO index (i.e., the time series associated with the first EOF of the 7-yr low-pass-filtered annual SST computed over the Pacific region; from 30°S to 63°N). The phase represented here is conventionally known as the negative phase of the IPO. Also shown is the regression on the IPO index of the DJFM mean Z500 (contours; units are meters per std dev of the IPO index, with interval of 1.5 m from -9 to $+9$ m). All variables have been 7-yr low-pass filtered prior regression.

The simulated seasonal variations of the AMV over the SPG region bear some resemblance with the seasonal cycle of the observed AMV as estimated by Ting et al. (2014; cf. Fig. 8 in their paper). That is, during JJAS two anomaly maxima can be seen, one southeast of the Greenland tip and another one east of the Grand Banks; during DJFM a maximum is located east of the Grand Banks (especially in CM2.1), whereas a minimum is seen over the Labrador Sea. This suggests that the seasonal cycle of the mixed layer depth may contribute to the seasonal modulation of the observed AMV.

Outside of the North Atlantic, the two models agree quite well on the global impacts of the AMV. Both models simulate a slight warming of the Indian Ocean and a negative phase of the IPO over the Pacific. They show a warming of about 0.3°C over Mexico and the eastern part of United States, a warming over eastern Brazil, and positive anomalies over the Mediterranean area and over southern Asia, with a warming reaching up to 0.4°C over the Himalayan plateau in CESM1. The models also agree on the simulated warming over Siberia and on the cooling of the northwestern part of North America, but these anomalies are only significant in CM2.1. AMV+ drives a cooling of the northern part of South America and Australia, which contrast with the warming seen in JJAS over these regions. As for the JJAS season, CESM1 simulates a significant warming of the Arctic that is only found in the northeastern rim of Siberia in CM2.1.

We find that the AMV leads to significant changes in the atmospheric winter circulation also as illustrated by the SLP and precipitation anomalies (Figs. 4c–f). A northward shift of the ITCZ and a southwestward shift of the SPCZ are again found over the tropical band, together with reduced pressure over the tropical

Atlantic and increased pressure over the Pacific. These features are coherent with the La Niña-like temperature pattern seen in Figs. 4a,b. In addition, both models simulate a precipitation decrease over Mexico and over the southern United States.

Over the North Pacific, the AMV leads to a weakening of the Aleutian low associated with an east–west dipole in the precipitation anomalies over the North Pacific. The North Pacific SST response is also consistent with the Aleutian low weakening as discussed by Zhang and Delworth (2015). In their study they linked a northward shift of the westerlies to a northward shift of the oceanic gyre circulation through a Sverdrup balance and to the propagation of oceanic Rossby waves from the central Pacific to the western coast, explaining the warmer SST off Japan. Over the northeastern side of the North Pacific, the SST cooling is driven by an anomalous advection of cool air from the Arctic. The decrease of the Aleutian low is paired with negative SLP anomalies over the Arctic centered northeast of Siberia. This whole North Pacific SLP response is similar to the one observed during La Niña events (cf. Fig. 2 in Trenberth et al. 1998). Furthermore, the precipitation and SLP signals are reminiscent of those documented in the “water hosing” experiments of Zhang and Delworth (2005), Dong and Sutton (2007), and Okumura et al. (2009), although the impacts are weaker in our experiments as expected from the weaker imposed forcing.

While the North Pacific response is quite similar in CM2.1 and CESM1, the North Atlantic response is notably different. CESM1 simulates an increase of precipitation over southern Europe associated with a north–south dipole of SLP anomaly that bears some resemblance to the NAO in its negative phase (NAO–). The SLP anomalies in CM2.1 do not project strongly

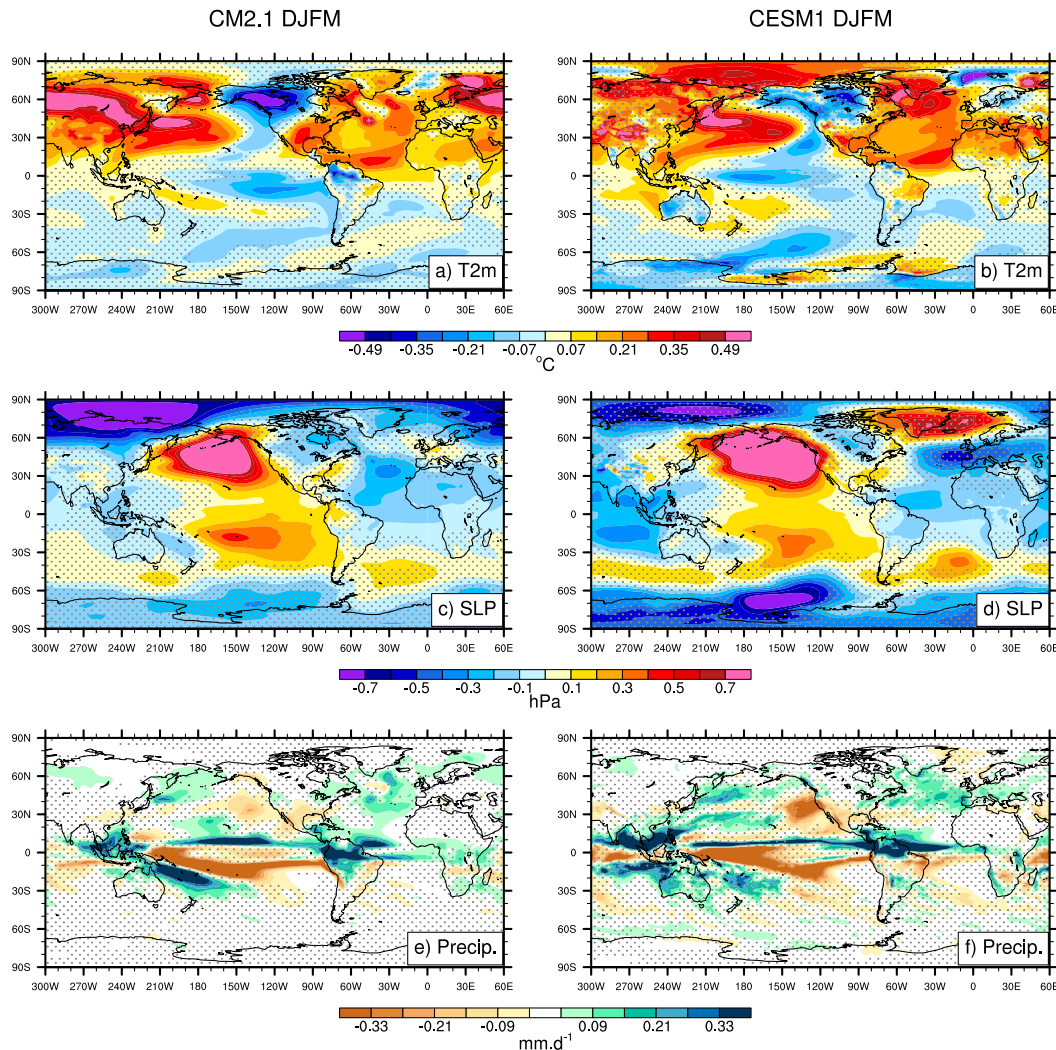


FIG. 4. As in Fig. 2, but for the DJFM season.

onto the NAO, even though negative SLP anomalies are present over the Azores. Assuming a barotropic atmospheric response to the AMV, one would expect anomalies in the geopotential height at 500 hPa (Z500) of the same sign as the SLP anomalies. However, the Z500 shows only weak negative and statistically insignificant anomalies around the Azores in both models (Figs. 5, 6b, and 7b). In CESM1, only the positive Z500 anomalies centered over Greenland and Iceland are statistically significant. In CM2.1 there are positive Z500 anomalies centered over the northwest of the United Kingdom, which project onto a negative phase of the east Atlantic pattern (EAP⁻; the EAP is defined in observations as the second mode of variability of the atmosphere over the NAE region; e.g., Barnston and Livezey 1987). The different patterns between SLP and Z500 anomalies over the extratropics can partially be

explained by the thermal expansion of the lower troposphere associated with the large-scale warming of the surface temperature.¹ To reduce this thermal effect on Z500 we subtract its zonal mean and focus on Z500* (asterisk denotes the departure from the zonal average). The Z500* anomalies in CESM1 clearly project onto an NAO⁻ (Fig. 5b). For CM2.1 this diagnostic suggests that the NAE atmospheric response might project onto a mix of both an NAO⁻ and an EAP⁻ (Fig. 5a). Despite the different patterns, for both models the atmospheric response to the AMV tends to decrease the

¹ This expansion leads to positive Z500 anomalies as well as to a divergence on average over the atmospheric column, which yields negative SLP anomalies. This large-scale adjustment can mask the atmospheric dynamical response to the North Atlantic warming.

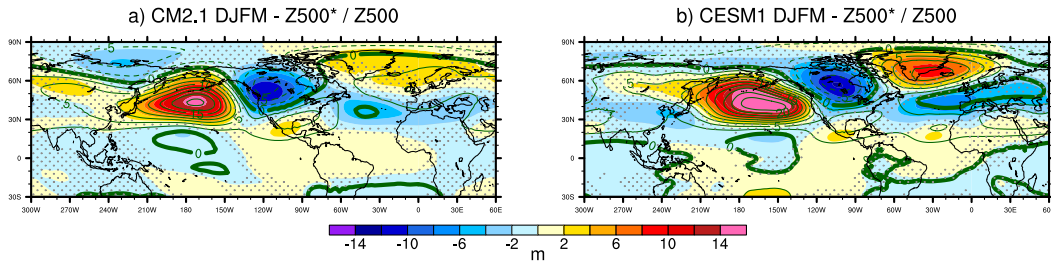


FIG. 5. Difference between the 10-yr average of the Full_AMV+ and the Full_AMV– ensemble simulations for the DJFM season for Z500 (contour interval of 2.5 m) and the departure of Z500 from the zonal mean (Z500*; color shading) for (a) CM2.1 and (b) CESM1. Stippling indicates regions that are below the 95% confidence level of statistical significance for the Z500* anomalies.

westerly atmospheric mean flow over the NAE region and thereby decrease the mean advection of relatively warmer oceanic conditions over land during winter, which is consistent with the study of Yamamoto and Palter (2016) based on observations. This may explain the absence of significant positive 2-m temperature (T2m) anomaly over central Europe in our simulations.

We have verified that the nature of the CM2.1 atmospheric response described above and hence its differences from the winter CESM1 atmospheric response are only marginally impacted by the North Atlantic SPG drift in CM2.1 as described in section 2b (cf. Fig. S5 in the supplementary material). It is then very likely that the different amplitude and structure of the atmospheric

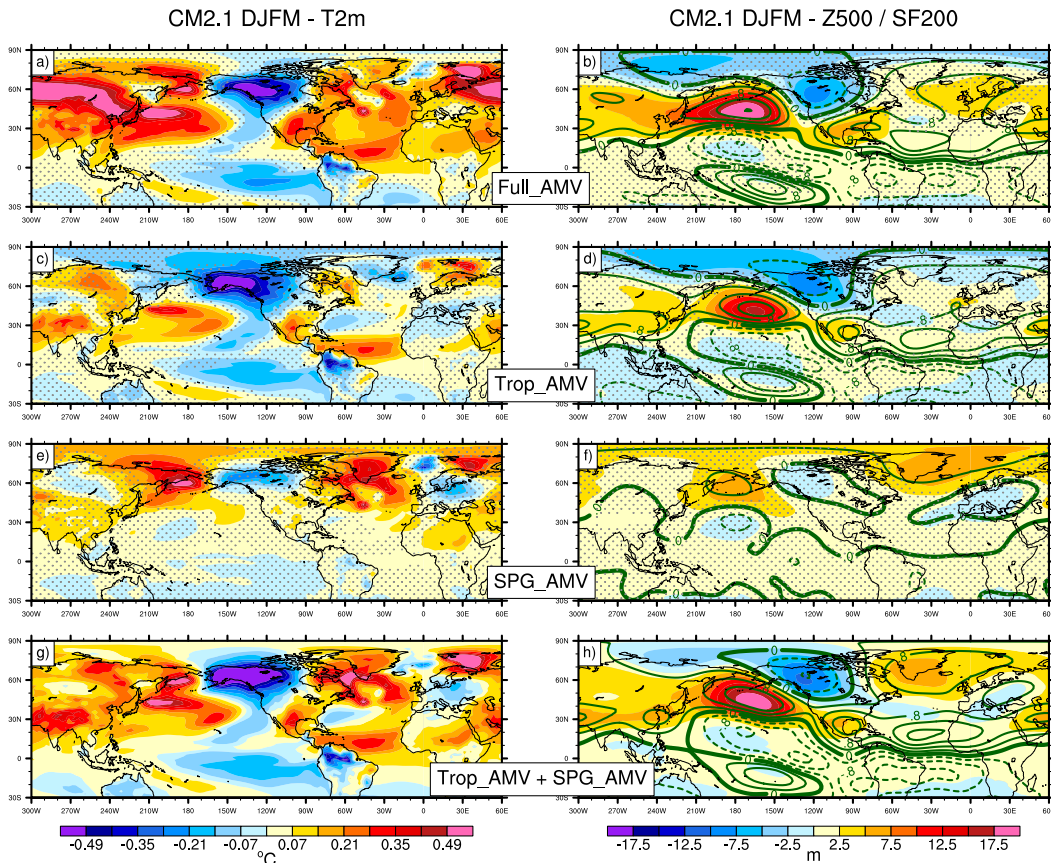


FIG. 6. Difference between the 10-yr average of the positive and the negative phases of (a),(b) Full_AMV, (c),(d) Trop_AMV, (e),(f) SPG_AMV, and (g),(h) sum of the Trop_AMV and SPG_AMV fields for CM2.1 in DJFM. (left) T2m (color shading) and (right) Z500 (color shading) and SF200 (contour interval of $0.4 \times 10^6 \text{ m}^2 \text{ s}^{-1}$). Stippling indicates regions that are below the 95% confidence level of statistical significance.

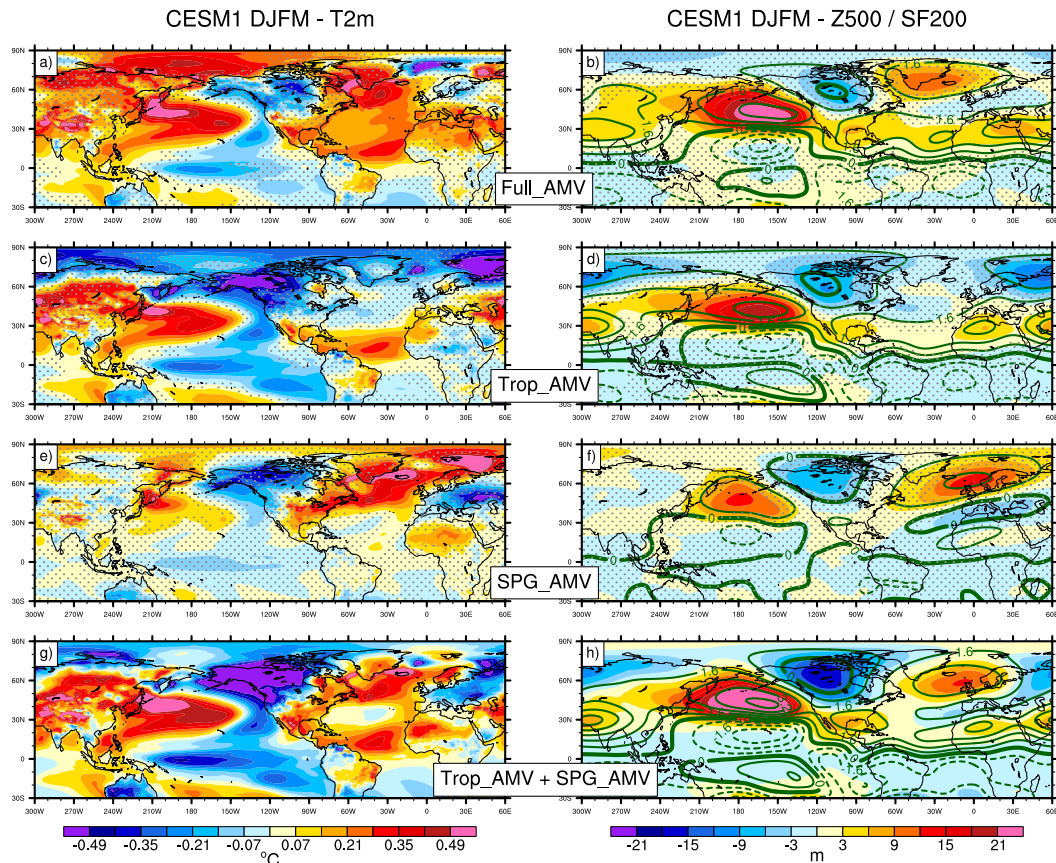


FIG. 7. As in Fig. 6, but for CESM1. Note that the Z500 contour intervals are different than in Fig. 6 and that the SF200 contours are plotted at intervals of $0.8 \times 10^6 \text{ m}^2 \text{ s}^{-1}$.

response between the two models are due to different sensitivities to the AMV forcing as discussed later.

Over the Pacific, both CM2.1 and CESM1 show Z500 anomalies reminiscent of the negative phase of the Pacific–North American pattern (PNA; e.g., Barnston and Livezey 1987), with positive Z500 anomalies centered over the Aleutian low and Mexico and negative anomalies centered over Canada and south of Hawaii. The latter center of action is more visible when looking at the anomalies of the streamfunction at 200 hPa (SF200; Figs. 6b and 7b), and it suggests a link between the tropical Pacific response and the PNA signal through tropical–extratropical teleconnections. This will be discussed in the next section.

4. Origins of the AMV climate impacts and associated mechanisms

a. Tropical versus extratropical contribution to the AMV climate impacts

We investigate the respective contribution of the tropical and extratropical parts of the AMV to the

climate impacts described in section 3 by performing two additional sets of experiments in which only the subpolar (SPG_AMV) or the tropical (Trop_AMV) part of the AMV pattern is imposed (cf. section 2b for the experiment details). We find that in both models, the Pacific IPO-like and PNA-like responses are primarily driven by the tropical part of the AMV (Figs. 6c,d and 7c,d). This result corroborates the studies of Kucharski et al. (2015) and McGregor et al. (2014), who highlighted that the tropical Pacific cooling observed during the last decades was forced by the tropical Atlantic warming through a modification of the WC. It is also consistent with the study of Zhang and Zhao (2015), who highlighted the link between the tropical Atlantic and the Pacific Ocean in the context of mean model biases. In line with Sutton and Hodson (2005), we find that the AMV impacts over the Americas are mainly explained by the tropical part of the AMV but that they are reinforced by the subpolar part of the AMV (Figs. 6e and 7e), especially over North America in CESM1.

Both models show marginal impacts over North Africa and Europe in terms of T2m anomalies in

response to the tropical AMV anomalies only, whereas a warming of North Africa and a cooling of Europe is simulated in both models in response to the SPG anomalies. This cooling is consistent with the Z500 dipole anomaly seen in both models over the NAE region, which tends to decrease the atmospheric flow blowing from the relatively warm ocean to the relatively cool continent in winter. This atmospheric response is in line with the study of [Gastineau and Frankignoul \(2012\)](#), who pointed to the importance played by the subpolar gyre anomalies in the atmospheric response to the AMOC decadal variability. Yet, in their study, the North Atlantic atmospheric response projects onto the NAO, whereas in our SPG_AMV the Z500 dipole response is shifted eastward compared to the model NAO.² The eastward-shifted Z500 dipole is, however, consistent with the atmospheric response found by [Peings and Magnusdottir \(2015\)](#) when they prescribe a surface AMV-like forcing in an atmospheric model coupled to a slab ocean (cf. Fig. 2 in their paper).

The SPG_AMV experiment generates a strikingly larger atmospheric response in CESM1 than in CM2.1. For the former, we note that the subpolar gyre part of the AMV leads to impacts that are weaker but similar in pattern to those driven by the tropical part of the AMV in terms of T2m and Z500 over the North Pacific region, which is consistent with the weak but significant warming simulated in the tropical North Atlantic in the CESM1 SPG_AMV experiment. This suggests that part of the tropical signature of the AMV could be forced by the subpolar part of the AMV as suggested by [Dunstone et al. \(2011\)](#) and [Smirnov and Vimont \(2012\)](#).

The cooling over Europe simulated by the SPG_AMV experiments contrasts with the slight warming simulated in the Full_AMV experiments. This discrepancy can be explained by the fact that our definition of the tropical and subpolar domains does not cover the whole North Atlantic when summing up the two regions; specifically, the subtropical North Atlantic ($\sim 25^{\circ}$ – 40° N) warming is not prescribed in either Trop_AMV or SPG_AMV, while it is included in Full_AMV. To test this hypothesis, we performed an additional experiment with CM2.1 called XTrop_AMV in which the AMV SSTs are imposed over the 28° – 73° N region (cf. [section 2b](#)). The XTrop_AMV experiment shows impacts over Europe of opposite sign to those simulated in the SPG_AMV experiments (Fig. S6 in the supplementary material), indicating that the 25° – 40° N latitude band of the AMV

may contribute to the European warming seen in Full_AMV. Yet, in XTrop_AMV, the imposed anomalies north of 28° N tend to propagate over the tropical Atlantic. Therefore, we cannot fully attribute the differences of climate responses between XTrop_AMV and SPG_AMV experiments to the 25° – 40° N latitude band forcing. There could also be nonlinear processes at play when the atmosphere is constrained by both the tropical and the subpolar gyre SSTs.

To further test whether the response to the tropical and extratropical forcings associated with the AMV are linear, we compare the sum of the Trop_AMV and SPG_AMV experiments (Figs. 6g,h and 7g,h) with the Full_AMV experiments (Figs. 6a,b and 7a,b). We find that the NAO-like response present in the CESM1 Full_AMV experiment is not reproduced by the sum of the SPG_AMV and Trop_AMV experiments. This suggests that both the tropical and the extratropical parts of the AMV are needed to force an NAO response in CESM1. While such nonlinearity of the atmospheric response to the AMV forcing in the NAE region is consistent with the findings of [Peings and Magnusdottir \(2015\)](#), it is in contrast with the study of [Davini et al. \(2015\)](#), suggesting model dependency of the response. The linearity of the impacts does not hold for the Arctic temperature response in CESM1 either, possibly because—when applying together—the SPG forcing is amplified by the tropical AMV forcing in this model. A similar statement can be made for the temperature response over the Eurasian continent in CM2.1, for which the Full_AMV experiment tends to show warmer conditions than the sum of Trop_AMV and SPG_AMV.

We showed previously that the tropical part of the AMV leads to a Pacific response that projects onto the IPO and PNA. This result contrasts with the [Zhang and Delworth \(2007\)](#) study, in which it was argued that the AMV impacts the PNA and the northern part of the IPO through teleconnections between the extratropical Atlantic and the extratropical Pacific. They stated that the extratropical North Atlantic warming associated with AMV+ leads to a weakening of the northward atmospheric momentum transport driven by the eddy activity over all Northern Hemisphere midlatitudes. We investigate this potential teleconnection by looking at the storm-track response (Fig. 8). Over the North Atlantic, there is no significant signal in the Full_AMV experiments in either model (Figs. 8a,b). This contrasts with the modeling studies of [Zhang and Delworth \(2007\)](#), [Peings and Magnusdottir \(2015\)](#), and [Davini et al. \(2015\)](#), who find a strong North Atlantic storm-track response to the AMV forcing. Over the North Pacific, there is a northward shift of the storm track in both models as found by [Zhang and Delworth \(2007\)](#).

² Pattern correlation of -0.50 and -0.25 for CM2.1 and CESM1 over the NAE region for the NAO pattern defined as the first EOF of Z500 over the same NAE region.

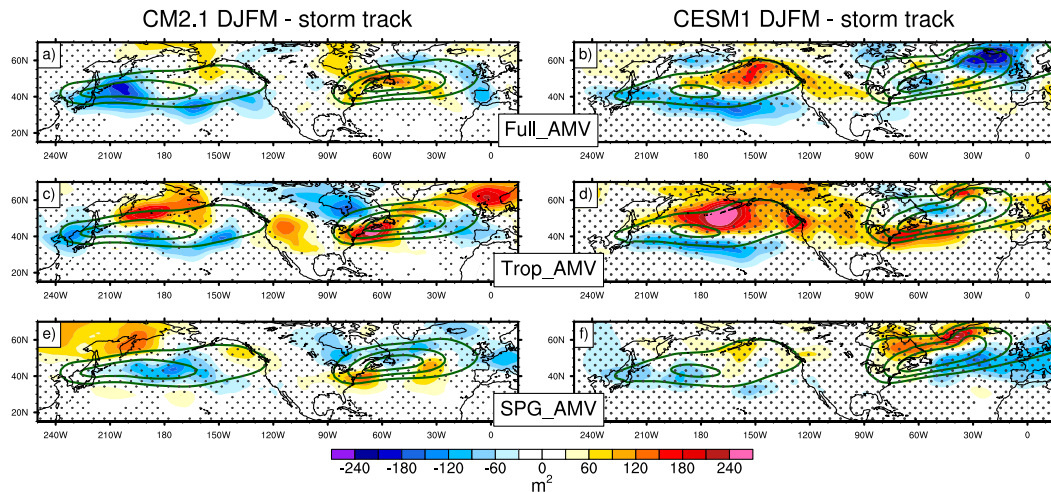


FIG. 8. DJFM season difference of the 8-day high-pass-filtered 500-hPa geopotential height variance (proxy of the atmospheric eddy activity; color shading) between the 10-yr average of (a),(b) the Full_AMV, (c),(d) the Trop_AMV, and (e),(f) SPG_AMV experiments. Results from (left) CM2.1 and (right) CESM1 are shown. Stippling indicates regions that are below the 95% confidence level of statistical significance. The climatological atmospheric eddy activity is overlaid in all panels (contour interval of 1000 m^2 from 2500 to 5500 m^2).

However, our results suggest that such a shift is weak and only marginally significant. This storm-track response appears to be driven in both models by the tropical part of the AMV (Figs. 8c,d) rather than the extratropical part (Figs. 8e,f). Therefore, we conclude that Zhang and Delworth (2007)'s mechanism is not at play here. We further conclude that the North Pacific storm-track response seen in our Full_AMV experiments should be interpreted as a consequence of the atmospheric mean-state changes (cf. Figs. 6b and 7b; i.e., the interaction between the background flow and the storm track activity, consistent with the canonical storm-track response observed during ENSO events; e.g., Seager et al. 2010b).

b. Influence of ocean dynamics and low-frequency air–sea coupling on the simulated AMV impacts

To estimate the importance played by the ocean in determining the climate impacts of the AMV, we perform an experiment similar to the Full_AMV experiment but in which the SSTs outside of the North Atlantic are restored to their own climatology: the Damped_Global_AMV experiment (cf. section 2b). The T2m anomalies and the Z500 anomalies simulated by Damped_Global_AMV (Figs. 9c,d) show patterns extremely similar to those in Full_AMV albeit with much reduced amplitude (Figs. 9a,b), suggesting that the structure of the primary large-scale climate impacts of the AMV can be broadly reproduced without ocean dynamics. In particular, the PNA-like signal is present in Damped_Global_AMV but strongly diminished compared to the

Full_AMV case, indicating that this response is amplified by oceanic processes.

Over the North Atlantic, Damped_Global_AMV simulates an atmospheric response that projects onto an NAO– pattern.³ This signal contrasts with the EAP-like anomalies seen in Full_AMV, and it demonstrates that in CM2.1, the direct effect of the AMV on the NAE atmosphere (i.e., the NAO anomaly) is modified by the remote effects of the AMV on other oceanic basins (e.g., the tropical and North Pacific responses). To better understand the direct local response to the AMV (i.e., the response that is not perturbed by remote teleconnections), we compare the Damped_Global_AMV experiment with the SPG_AMV ones. In the latter almost no atmospheric anomalies were visible outside of the North Atlantic (Fig. 6f), suggesting only a direct impact of the AMV forcing. However, the atmospheric signal over the NAE region was shifted eastward compared to the Damped_Global_AMV case. This suggests that both the SPG and the tropical part of the AMV contributes to the NAO response in Damped_Global_AMV and that it is in addition modified by the remote atmospheric response of the Pacific to the tropical part of the AMV in the Full_AMV experiments. Indeed, the

³ Correlation map coefficient of 0.78 (0.56) over the NAE region with the NAO pattern defined as the first EOF of Z500 over the same region after (before) removing the thermal expansion of the atmosphere. This is removed here by subtracting from each grid point the spatial average of Z500 over the NAE region.

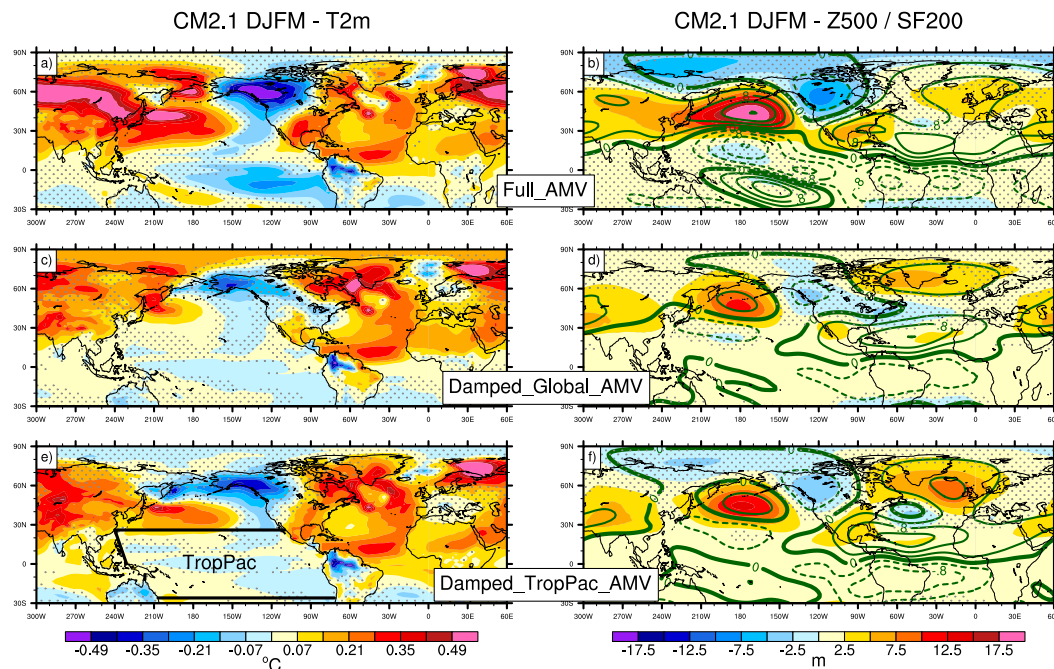


FIG. 9. As in Fig. 6, but for (a),(b) Full_AMV, (c),(d) Damped_Global_AMV, and (e),(f) Damped_TropPac_AMV experiments of CM2.1 during DJFM. The black lines in (e) outline the tropical Pacific domain restored to its climatology in the Damped_TropPac_AMV experiments.

regression map of Z500 on the IPO index⁴ shows that the negative phase of the IPO is associated with negative Z500 anomalies over Greenland (Fig. 3; i.e., the opposite atmospheric response to that shown in the Damped_Global_AMV experiment).

c. Role of the tropical Pacific in the simulated AMV climate impacts

We investigate here the mechanism through which the tropical part of the AMV leads to a PNA-like response over the North Pacific. Previous studies suggest that this teleconnection can occur either by westward propagation of atmospheric Rossby waves from the tropical Atlantic to the North Pacific (e.g., Lee et al. 2009) or through atmospheric changes in the tropical Pacific (e.g., Horel and Wallace 1981). The latter would imply first a modification of the WC that would lead to tropical Pacific rainfall anomalies. The heat anomalies associated with these precipitation changes would then generate a tropical–extratropical Rossby wave propagation in the Pacific, with a structure that projects on the PNA. Given the strong ocean–atmosphere coupling in the tropical Pacific, preventing SST anomalies there reduces the

atmospheric response. Hence, to test the second mechanism we analyze the Damped_TropPac_AMV experiments (Figs. 9e,f; cf. section 2b). We find that the magnitude of the PNA response in this experiment is about 35% smaller than that of the Full_AMV experiment [-0.146 vs -0.095 as estimated by the PNA index definition of Wallace and Gutzler (1981)]. The stronger PNA signal in Full_AMV implies that part of this AMV teleconnection is relayed by the tropical Pacific response. The PNA amplitude in Damped_TropPac_AMV is, however, stronger than in the Damped_Global_AMV experiments, the latter having a PNA index value of -0.061 (i.e., 60% weaker than in Full_AMV). This indicates a positive feedback between ocean and atmosphere anomalies over the North Pacific and/or a role played by the Indian Ocean warming response. The former feedback is consistent with the study of Zhang and Delworth (2015), who highlighted the existence of a two-way coupling between the Pacific decadal oscillation (e.g., Newman et al. 2016) and the PNA.

5. Mechanisms of the tropical Pacific response

We investigate the mechanisms through which the tropical Pacific response to the AMV is set by looking at the transient response (month by month) in the

⁴The IPO time series corresponds to the principal component associated with the EOF shown in Fig. 3a.

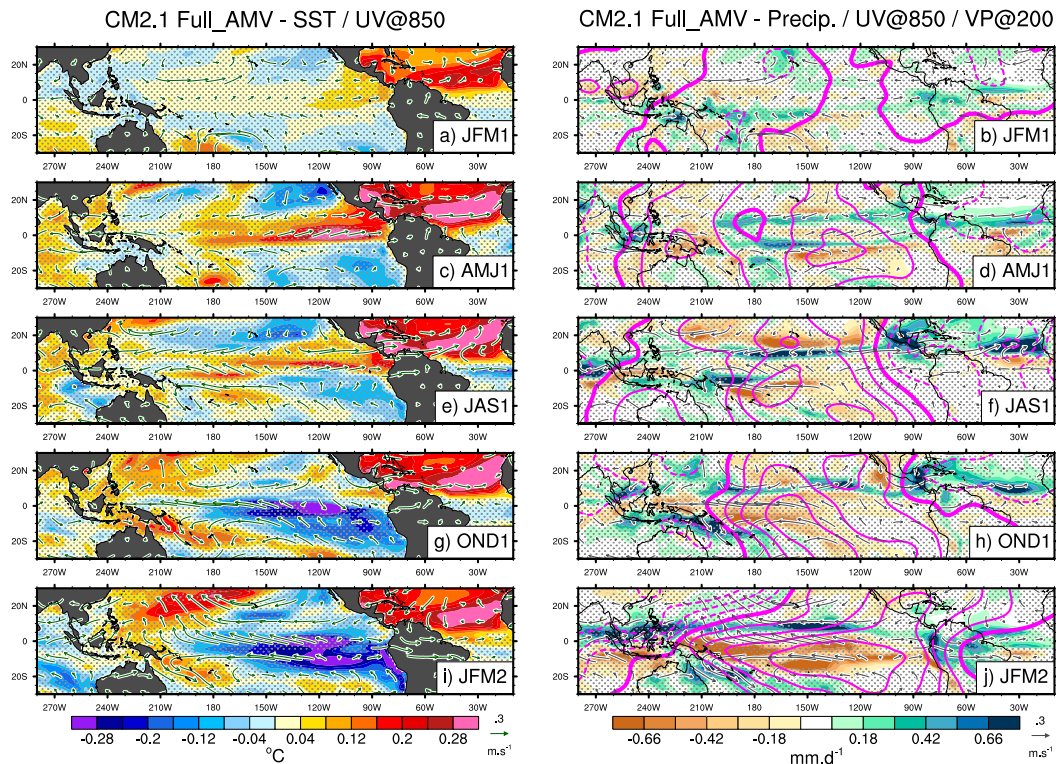


FIG. 10. Time evolution of the differences between Full_AMV+ and Full_AMV– from (top) JFM1 to (bottom) JFM2. (a),(c),(e),(g),(i) Sea surface temperature (color shading) and winds at 850 hPa (vectors) and (b),(d),(f),(h),(j) precipitation (color shading), velocity potential of the wind at 200 hPa (contour interval of $0.1 \times 10^6 \text{ m}^2 \text{ s}^{-1}$), and winds at 850 hPa (vectors). Stippling indicates regions below the 95% confidence level of statistical significance.

Full_AMV experiments. A slight warming can be seen over the eastern equatorial Pacific during January–March (JFM) and April–June (AMJ) of the first year (JFM1 and AMJ1; Figs. 10a,c and 11a,c). This comes from the turbulent surface heat fluxes (not shown) due to both the advection of heat anomalies from the Atlantic by the mean flow and the local decrease of the trade winds. In CM2.1, the equatorial Pacific warming is stronger than in CESM1, and it persists until the summer [July–September (JAS1)], extending to the western part of the Pacific. As the wind anomalies are similar between the two models, this suggests more atmospheric heat advection from the North Atlantic by the mean flow in CM2.1. This difference is consistent with the larger JJAS T2m response in CM2.1 (Fig. 2a) compared to that in CESM1 (Fig. 2b). In AMJ1, there is an increase of the trade winds over the western part of the Pacific that is reinforced in the following months (Figs. 10e,g,i and 11e,g,i). These wind anomalies are eventually associated with negative SST anomalies over the entire equatorial Pacific so that the two models simulate overall a La Niña–like pattern during the second boreal winter (Figs. 10g,i and 11g,i).

The strengthening of the western Pacific trade winds during AMJ1 and JAS1 is consistent with the changes of the WC diagnosed from surface wind, velocity potential at 200 hPa (VP200), and precipitation (Figs. 10d,f and 11d,f). Indeed, the tropical Atlantic warming enhances the atmospheric deep convection in the Atlantic. Similar to an atmospheric Gill–Matsuno response to a north equatorial forcing (e.g., see Gill 1980, their Fig. 3), this warming is able to excite an equatorial Kelvin wave east of the SST forcing, which is associated with easterly wind anomalies in the lower troposphere (cf. wind anomalies in Figs. 10e and 11e). West of the SST forcing, the warming excites Rossby wave packets associated with off-equatorial cyclonic flows in the lower troposphere around 20°N (cf. SLP anomalies around Mexico in Figs. 2c,d) and equatorial westerly wind anomalies (cf. wind anomalies in Figs. 10e and 11e). These results are consistent with Dong and Sutton (2002) and with the recent study of Li et al. (2015). The latter shows that when a tropical Atlantic warming is imposed in the dry dynamical core of the GFDL model (Held and Suarez 1994), the wind anomalies induced by the Rossby waves and the Kelvin waves lead to both a flow divergence in

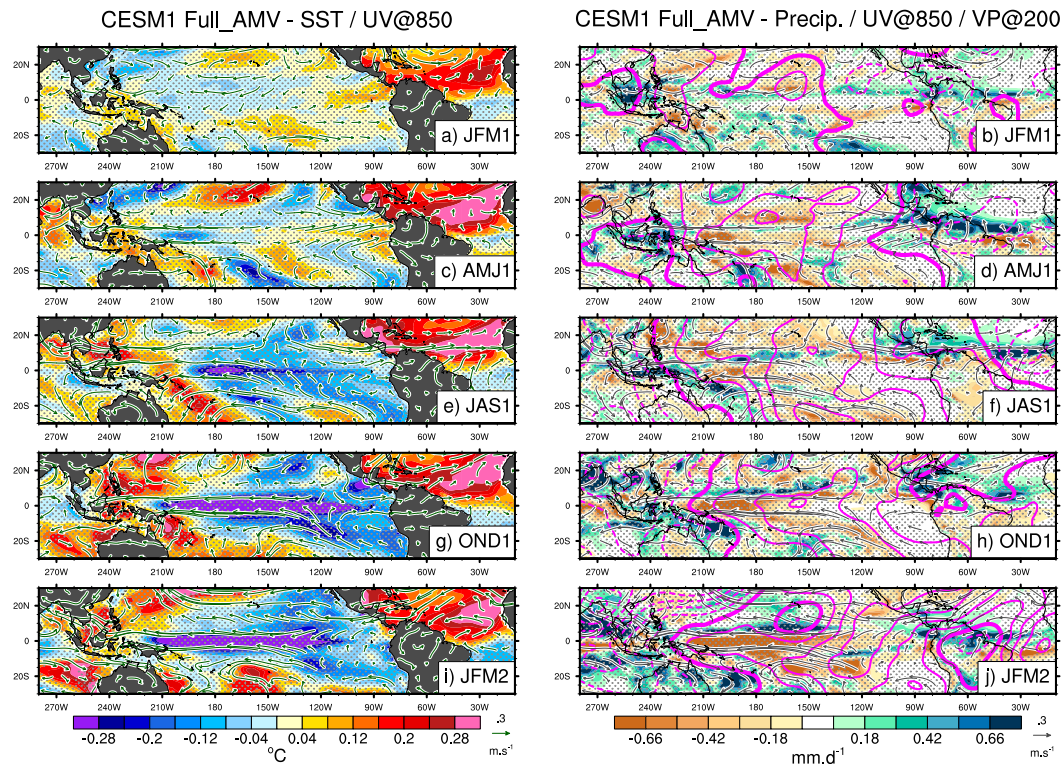


FIG. 11. As in Fig. 10, but for CESM1. The velocity potential of the wind at 200 hPa is plotted with contours at intervals of $0.15 \times 10^6 \text{ m}^2 \text{ s}^{-1}$.

the lower atmosphere and to a convergence in the upper atmosphere over the central Pacific (cf. Li et al. 2015; Fig. S5). The anomalous Walker cell is closed by a downward motion over the tropical Pacific, where it is associated with a precipitation decrease over the equator and over the southeast of the SPCZ.

From JAS1 to JFM of the second year (JFM2), the ascendant anomaly over the tropical Atlantic decreases (Figs. 10h,j and 11h,j). In contrast, the tropical Pacific subsidence and the precipitation anomalies remain and seem tightly linked to the reinforcement of the wind and of the SST anomalies there (Figs. 10g,i and 11g,i) and with the formation of a new anomalous ascendant zone centered over the northwest of the equatorial Pacific. This suggests an amplification of the tropical Pacific response to the direct North Atlantic impact through local feedbacks such as the Bjerknes feedback, the thermocline feedback, and the wind–evaporation–sea surface temperature (WES) feedback as documented in previous studies by Wu et al. (2005), Dong and Sutton (2007), Li et al. (2015), and Jia et al. (2016), among others. Detailed investigation of the relative role played by these different feedbacks would require further sensitivity experiments and is beyond the scope of this study. However, the differences in the SST anomalies

during JAS1 between CESM1 and CM2.1 (Figs. 10e and 11e) and the similarity of the wind anomalies suggest that the WES feedback is not the original player in the simulated amplification.

The Damped_Global_AMV experiments show similar impacts in JAS and October–December (OND) to the Full_AMV experiments (Figs. 12b,c) but much weaker anomalies in JFM (Fig. 12d). This confirms that the boreal winter La Niña–like pattern is not a direct impact of the AMV but an adjustment of the tropical Pacific to the AMV forcing during the previous boreal summer. Hence, we stress here that the Pacific adjustment to the tropical Atlantic forcing proposed by Li et al. (2015) has to be interpreted keeping seasonal adjustments in mind. This lagged teleconnection is in line with the seasonal link between Atlantic Niño–Pacific ENSO described by Rodríguez-Fonseca et al. (2009), Martín-Rey et al. (2014), and Polo et al. (2015).

Because there is no seasonal variation of the SST anomalies imposed over the tropical Atlantic in our experiments, the intermittence of the atmospheric bridge between the Atlantic and the Pacific must come from the seasonal evolution of the mean state. As stated by Sutton and Hodson (2007), we explain this seasonal dependency by higher seasonal mean SST anomalies in

CM2.1 Damped_Global - Precip. / UV@850 / VP@200

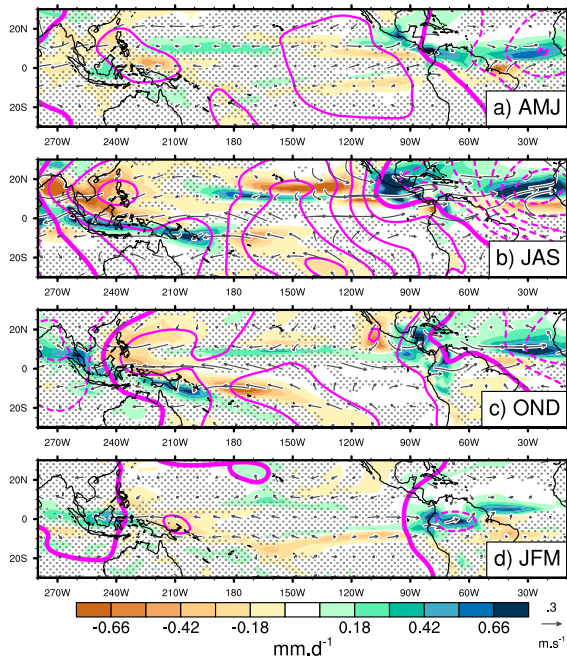


FIG. 12. Differences between the 10-yr mean of Damped_Global_AMV+ and Damped_Global_AMV− for (a) JFM, (b) AMJ, (c) JAS, and (d) OND of precipitation (color shading), potential velocity of the wind at 200 hPa (interval of $0.1 \times 10^6 \text{ m}^2 \text{ s}^{-1}$), and winds at 850 hPa (vectors). Stippling indicates regions below the 95% confidence level of statistical significance.

the northwestern tropical Atlantic between July and November than during other months. Over this period, small SST anomalies can have a strong impact on the atmospheric deep convection and on the generation of tropical atmospheric waves through the release of latent heat.

We further explore the tropical Pacific response by analyzing the amplitude of the ENSO response. This is investigated using the principal component associated with the first EOF of the upper-200-m oceanic heat content (HC200) computed over the tropical Pacific (30°S – 30°N) during DJFM (ENSO_PC). ENSO_PC captures the ocean dynamical characteristics of ENSO such as the deepening and seesaw of the tropical Pacific thermocline. We use this index rather than the well-known SST-based ENSO proxies such as the Niño-3 or Niño-3.4 indices because in our experiments these indices appear polluted by the atmospheric advection of heat anomalies from the Atlantic (cf. Figs. 10 and 11), and thus they do not properly represent the dynamical state of ENSO.

To illustrate the mean ENSO response to AMV forcing, we present in Figs. 13a,b the probability density function (PDF) of the ENSO_PC indices computed

Mean ENSO response

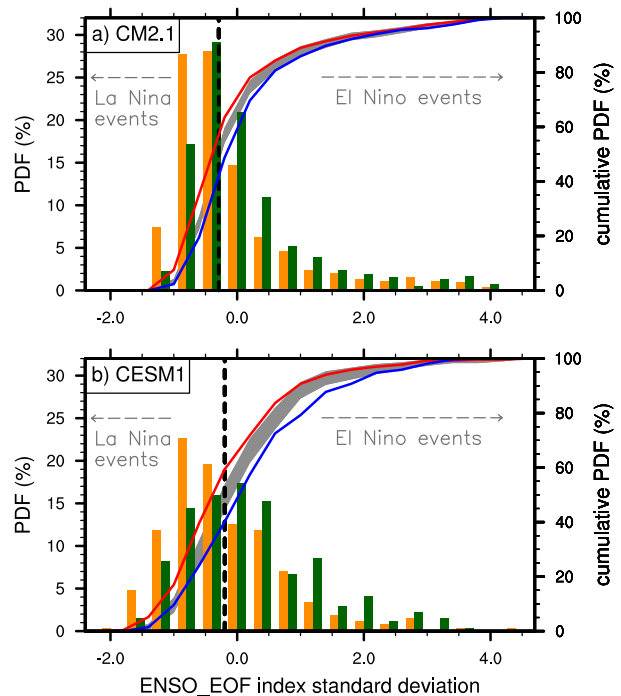


FIG. 13. PDF of the ENSO_PC index in the Full_AMV+ (orange histograms) and Full_AMV− (green histograms) experiments, built from the 10 DJFM values of all the ensemble members of (a) CM2.1 and (b) CESM1. Superimposed on each PDF is the cumulative PDF of the ENSO_PC index for the Full_AMV+ ensemble (red line) and the Full_AMV− ensemble (blue line). The gray shading indicates the 90% confidence interval in which the cumulative PDFs are not statistically different from what should be expected from the background noise of ENSO (based on a bootstrap sampling method). The vertical dashed line indicates the median value of the ensemble formed by all members of Full_AMV+ and Full_AMV−.

from the 10 years of the Full_AMV+ and Full_AMV− ensemble member simulations. To estimate how the mean-state changes project on ENSO, the EOF analysis is based on the covariance matrix computed from all members of both Full_AMV+ and Full_AMV−. The HC200 field of each member is then projected on the EOF pattern to obtain the corresponding ENSO index. Finally, PDFs of these ENSO indices are built separately for Full_AMV+ and Full_AMV− using all the DJFM values from each member. As expected by the negative SST anomalies seen in Figs. 10i and 11i, the ENSO PDFs exhibit a shift toward La Niña conditions in Full_AMV+ and toward El Niño conditions in Full_AMV−. Looking at the median value of the ensemble formed by both the Full_AMV+ and the Full_AMV− members (dashed vertical line on Figs. 13a,b), we can see that in the Full_AMV− case only 42%

(40%) of the members in CM2.1 (CESM1) are on the La Niña side against 57% (60%) in the Full_AMV+ case for CM2.1 (CESM1). If we consider the minus one standard deviation of the ENSO_PC index as the La Niña threshold, the PDF shift indicates about a doubling of La Niña events between Full_AMV– and Full_AMV+ (from 3% to 7% in CM2.1 and from 10% to 18% in CESM1). For CESM1, changes occur in the warm phase of ENSO as well with a doubling of the frequency of occurrence of El Niño events between Full_AMV+ and Full_AMV– (taking plus one standard deviation of the ENSO index as the El Niño threshold). For CM2.1, however, the shift is not as marked, with an increase of the frequency of El Niño events by a factor of 1.3. Such modulation of the tropical Pacific interannual variability by the AMV is consistent with the model studies of [Timmermann et al. \(2007\)](#) and [Dong and Sutton \(2007\)](#), who show an increase of the strength and of the occurrence of El Niño events following a shutdown of the AMOC in water hosing experiments.

6. SNR of the AMV response

The relative importance of the AMV impacts described earlier in the paper is assessed in this section by comparing each to the climate background variability. [Sutton and Hodson \(2007\)](#) used a signal-to-noise ratio (SNR) metric to quantify the relative strength of the AMV impacts. They defined it as the mean difference between their AMV+ and AMV– simulations, divided by the interannual standard deviation. Here, we propose a different definition of the SNR in order to link directly this quantity to the predictability associated to the AMV impacts. We define the signal S as the square of half the difference between the Full_AMV+ and the Full_AMV– ensemble means:

$$S = \left(\frac{\text{AMV}+ - \text{AMV}-}{2} \right)^2, \quad (1)$$

where

$$\text{AMV}+ = \frac{1}{n/2} \sum_{i=1}^{n/2} (x_i^+) \quad \text{and} \quad (2)$$

$$\text{AMV}- = \frac{1}{n/2} \sum_{i=1}^{n/2} (x_i^-). \quad (3)$$

The variables x^+ and x^- represent the value of the field (e.g., T2m) in each member of the Full_AMV+ and the Full_AMV– experiments, respectively, and $n/2$ is the number of ensemble members in each experiment. The

noise N is defined as the variance of the pool formed by all members of Full_AMV+ and Full_AMV– together:

$$\begin{aligned} N &= \frac{1}{n-1} \sum_{j=1}^n (x_j - X)^2 \\ &= \frac{1}{n-1} \left[\sum_{i=1}^{n/2} (x_i^+ - X)^2 + \sum_{i=1}^{n/2} (x_i^- - X)^2 \right], \quad (4) \end{aligned}$$

where X is the average between the Full_AMV+ and the Full_AMV– ensemble means:

$$X = \frac{\text{AMV}+ + \text{AMV}-}{2}. \quad (5)$$

Doing so, the SNR is equivalent to a variance ratio, where the signal is the interensemble variance, and the noise is the sum of the interensemble and the intra-ensemble variances.⁵ It can then vary between 0 and 1, 0 meaning no signal and 1 meaning that the entire variance is explained by the difference between the two ensemble means, which is the way we defined the response in the paper. An average over the 10 years of the simulations is performed before computing the noise in order to compare the AMV impacts with the decadal variability of the climate system. We stress here that this SNR represents a percentage of decadal time-scale variance. Hence, if an AMV impact over a region has an SNR of 0.2 associated with a decadal variance of 1°C^2 , this indicates that the AMV impact accounts for about 0.45°C (i.e., $\sqrt{0.2} \times \sqrt{1}$) of the 1°C anomaly. Furthermore, one can predict 20% of the variance of the decadal fluctuations over this region, assuming a complete predictability of the AMV. From this perspective, we stress that the SNR computed here is an upper bound of the predictability associated with the AMV impacts.

[Figure 14](#) shows the SNR associated with the AMV impacts in terms of T2m during the JJAS season at decadal time scale. By construction, the SNR of T2m shows strong values over the whole North Atlantic. We stress that our protocol allows us to estimate the SNR and the predictability of the AMV impacts and not that of the AMV itself, as the North Atlantic SSTs are constrained in our experiments. Outside of the North Atlantic region, the SNR in CESM1 is overall stronger than that of CM2.1. This comes from an overall stronger background noise in CM2.1 during JJAS over the Northern Hemisphere (not shown). High T2m SNR can be found in both models along the Kuroshio–Oyashio Extension, with values reaching up to 40% over the

⁵ This metric is also referred to in literature as the signal-to-total-variance ratio (e.g., [Tang et al. 2013](#)).

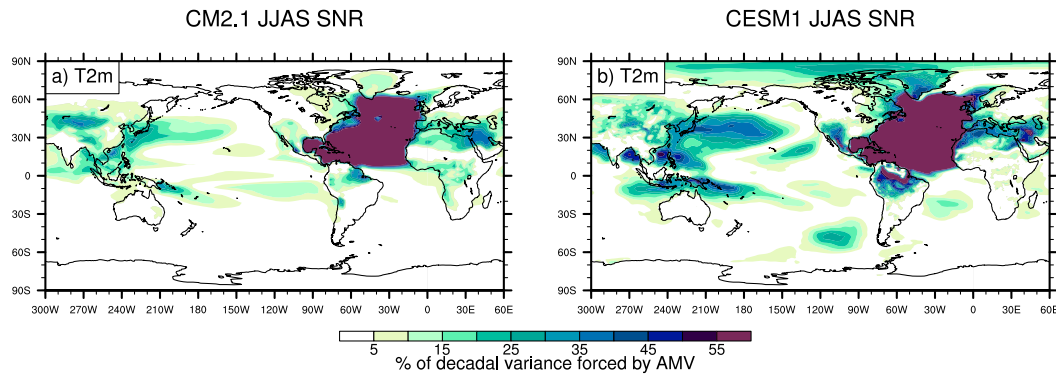


FIG. 14. SNR of the T2m anomalies from the Full_AMV experiments of (a) CM2.1 and (b) CESM1.

western part of the tropical Pacific in CESM1, suggesting a large predictability of the AMV impacts over the Pacific. Over land, the models show high predictability of the AMV impacts over northern South America, the Mediterranean basin, central Asia, and west of the United States. However, they show only weak SNR over most of the Southern Hemisphere.

During the DJFM season the T2m SNR over the Northern Hemisphere are weaker than during JJAS (Figs. 15a,b), which is coherent with the more chaotic behavior of the atmosphere during wintertime. We note also an absence of strong SNR over the western part of the North Atlantic SPG where the imposed signal is

weak (cf. Figs. 4a,b), which coincides with the region where the SST restoring is weak as a result of wintertime deep mixed layers. Both models show relatively high T2m SNR over the western part of the North Pacific ($>20\%$) as well as over the equatorial Pacific ($>15\%$) consistent with the ENSO response documented in section 5. CESM1 shows values of 20%–30% over the Mediterranean region and over the Maritime Continent, whereas the SNR in CM2.1 is almost zero over these regions. Over land, both models show an SNR of about 10% over Southeast Asia and 20%–25% over Mexico. Finally, it is important to point out that the SNR of T2m suggests only weak decadal predictability of the AMV

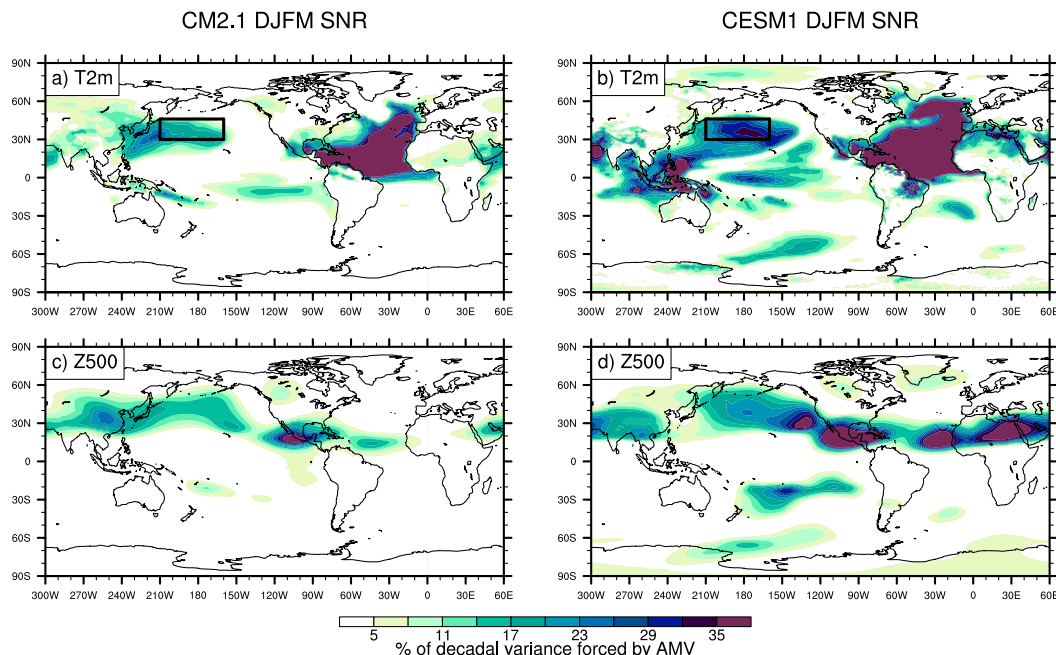


FIG. 15. SNR of (a),(b) the T2m anomalies and (c),(d) the Z500 anomalies from the Full_AMV experiments. Results from (left) CM2.1 and (right) CESM1 are shown. [The black rectangles in (a) and (b) show the northwestern Pacific domain used for the SST index of Fig. 16.]

impacts over land in the extratropics, with values representing overall less than 8% of the decadal variance. As expected from the stronger Z500 response in CESM1 compared to CM2.1 (Figs. 6b and 7b), the Z500 SNR is overall higher in CESM1 (Figs. 15c,d). It shows predictability of the AMV impacts over a broad Northern Hemisphere subtropical region extending between the eastern Pacific and East Asia. Over the extratropics, high SNR values are present around the Aleutian low, but the SNR is very small over the NAE region especially in CM2.1, indicating weak predictability of the AMV impacts over this region.

To further emphasize the importance of the AMV forcing on the North Pacific decadal variability, for all the Full_AMV+ and Full_AMV− ensemble members, we consider an index constructed as the spatially averaged SST over the northwestern Pacific region (NW_Pac; cf. limits on Figs. 15a,b) using 10-yr averages. Then, we compute all the possible combinations of the difference between the NW_Pac indices of the Full_AMV− members and the Full_AMV+ members and build the PDF of these combinations of the difference (Fig. 16). The PDF shows in more than 77% and 84% of the cases in CM2.1 and CESM1, respectively, the northwestern Pacific SSTs of Full_AMV− members are cooler than those in the Full_AMV+ members. We find that the mean difference for both models is about -0.3°C . In comparison, the observed difference of the northwestern Pacific SST associated with the well-documented regime shift that took place during the winter of 1976/77 in the North Pacific (e.g., Hare and Mantua 2000; Minobe 1999) was 0.4°C (dashed vertical line), as diagnosed by the difference between the 1977–86 and the 1967–76 periods. This climate shift caused considerable impacts on the physical and biological conditions leading to severe distribution and abundance changes of plankton and fish species (Ebbesmeyer et al. 1991; Mantua et al. 1997; Minobe 1997; Overland et al. 2008). Human impacts were substantial and came mainly through changes in North Pacific fisheries. This comparison shows that if our experiments represent nature closely enough, such a Pacific shift has a 40% chance to occur following an AMV transition from a positive to a negative phase.

7. Conclusions

We have investigated the climate impacts associated with an estimate of the internal component of the observed Atlantic multidecadal variability (AMV) using the GFDL CM2.1 and the NCAR CESM1 coupled models by restoring their North Atlantic SSTs to observed anomalies. This coupled approach allows us to

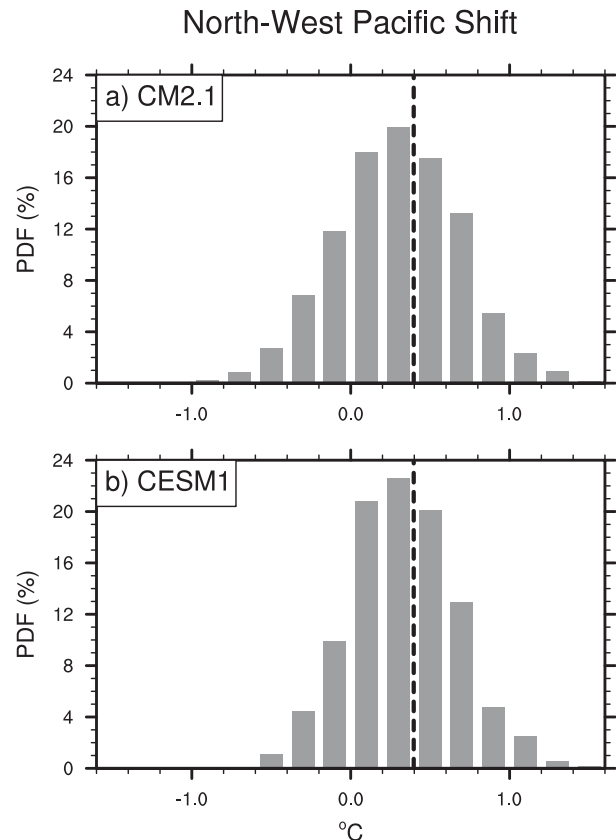


FIG. 16. PDF of the difference between the NW_Pac indices of the Full_AMV− and Full_AMV+ ensemble members from (a) CM2.1 and (b) CESM1. The dashed vertical line indicates the observed difference of the NW_Pac index between the 10-yr period after (1977–86) and the 10-yr period before (1967–76) the Pacific climate shift of 1976/77. The observed SST (ERSST.v3) difference is computed after removing the linear trend.

understand the full climate response to the imposed North Atlantic anomalies. During both boreal winter (DJFM) and boreal summer (JJAS), we find that the AMV can impact the climate of the entire globe. Our main findings are the following:

- 1) During JJAS, in both models the AMV warming drives a northward shift of the Atlantic intertropical convergence zone and a reinforcement of its northern branch. We showed that the diabatic heating anomaly associated with these precipitation changes leads to a modification of the Walker circulation (WC), with an anomalous rising branch over the North Atlantic and an anomalous sinking branch over the Pacific, in accord with previous studies by Dong et al. (2006), Kucharski et al. (2011), and McGregor et al. (2014). This perturbed WC generates precipitation anomalies over the whole tropical belt, strengthening monsoon activities over Asia and

Africa as previously found by the model study of [Zhang and Delworth \(2006\)](#). We show that the AMV warming also leads to reduced rainfall over the western part of the United States and to a north–south dipole of precipitation over Europe, indicating the AMV has played a role in the global climate variability observed during the last century. The latter impacts are consistent with previous observational and modeling studies by [Sutton and Hodson \(2005\)](#), [Wang et al. \(2008\)](#), [Schubert et al. \(2009\)](#), [Kushnir et al. \(2010\)](#), and [Sutton and Dong \(2012\)](#), suggesting that these are robust impacts of the AMV.

- 2) For the DJFM season, we find that the AMV modulates by a factor of about 2 the frequency of occurrence of El Niño or La Niña events in both the GFDL and NCAR models. This response is associated with broad Pacific anomalies that project onto the interdecadal Pacific oscillation (IPO) in its negative phase in response to the imposed tropical AMV warming. We show that this response comes from a modification of the WC during summer, which leads to the development of La Niña–like conditions during the following winter through processes that are associated with the Pacific internal variability as documented in [Li et al. \(2015\)](#). This lagged response of the tropical Pacific to the tropical Atlantic is consistent with the interseasonal triggering of La Niña onset by the Atlantic Niño recently documented in [Polo et al. \(2015\)](#).
- 3) In both models the northern part of the IPO-like SST response is tightly linked to a negative phase of the Pacific–North American teleconnection pattern (PNA). We show that the PNA-like response to the AMV is mainly driven by atmospheric teleconnections coming from the tropical Atlantic that are relayed and amplified by the tropical Pacific adjustment to the AMV forcing. No direct teleconnection between the extratropical Atlantic and the extratropical Pacific is present in our experiments, which contrasts with the study of [Zhang and Delworth \(2007\)](#), who argued for an extratropical teleconnection taking place through changes in the storm tracks.
- 4) We investigate the response of the North Atlantic–European (NAE) climate to the AMV and show that, despite the large-scale warming of the Northern Hemisphere continents simulated in both models during DJFM, no warming was present over central Europe. This absence of warming is consistent with the atmospheric response over the NAE region—and it projects on the negative phase of the North Atlantic Oscillation (NAO) for CESM1 and both on NAO– and on the negative phase of the east Atlantic pattern (EAP) for CM2.1. In both cases,

this atmospheric response reduces the westerly atmospheric mean flow and the associated advection of relatively warmer oceanic conditions over land during winter. This is in line with the recent study of [Yamamoto and Palter \(2016\)](#), who emphasized the lack of relationship between western Europe and the observed multidecadal fluctuations of the North Atlantic SSTs during the last century using a Lagrangian approach. However, the discrepancy of the NAE atmospheric response between the two models and the weak signal-to-noise ratio of the response reveal strong uncertainties of the AMV impacts over this region.

- 5) In both NCAR and GFDL models, the DJFM atmospheric circulation response over the NAE region is primarily driven by the subpolar part of the AMV, consistent with the AMOC impacts studied in [Gastineau and Frankignoul \(2012\)](#). However, in our experiments this response appears to be modified by the tropical AMV forcing. Specifically, we show that in CM2.1 the atmospheric response to the subpolar part of the AMV projects onto a negative NAO that is reinforced by the direct atmospheric response to the tropical part of the AMV. We show also that in our experiments, the NAE atmospheric response is eventually modified by the remote impacts of the tropical AMV forcing on the Pacific and ultimately it projects on both NAO– and EAP–.
- 6) The signal-to-noise ratio (SNR) of the air temperature suggests relatively high predictability of the AMV impacts during JJAS over the Mediterranean basin, central Asia, and the Americas from the United States to the north of South America. During DJFM the SNR shows only weak predictability over land. However, the large values and the agreement between the two models for the SNR of the temperature and the atmospheric circulation over the North Pacific, Mexico, and Southeast Asia indicates a high predictive skill of the AMV impacts over these regions during boreal winter.

8. Discussion

Our results stress the importance played by the North Atlantic Ocean variability associated with the AMV in driving changes at global scale, especially in the Pacific at the decadal time scale. Our conclusions are in line with the recent studies of [McGregor et al. \(2014\)](#), [Kucharski et al. \(2015\)](#), and [Li et al. \(2015\)](#). Interestingly, the AMV impacts in these studies are also similar to, although weaker than, the ones presented in the water hosing experiments of [Zhang and Delworth](#)

(2005), Dong and Sutton (2007), and Okumura et al. (2009), which documented the climate response following a dramatic slowdown of the AMOC. In the present study, we specifically focus on the climate impacts associated with an estimate of the internal component of the observed AMV, which has been shown to be predictable to some extent on multiyear-to-decadal time scale (e.g., Robson et al. 2012; Yeager et al. 2012; Msadek et al. 2014). Our results are therefore encouraging for the prospect of getting skillful decadal predictions over regions outside of the North Atlantic through the impacts of the AMV. The teleconnections we highlight between the Atlantic and the Pacific are also consistent with the studies of Chikamoto et al. (2012, 2015), who showed that phase shifts of the IPO as those observed in the late 1990s might be predicted few years in advance if the sign and amplitude of the AMV were to be predicted.

We further show in this study that most AMV global-scale impacts are driven by the tropical part of the AMV. Many studies that assessed decadal predictability using GCMs point out some predictability of the extratropical North Atlantic SSTs as a result of the potential predictability in AMOC variability, but the predictability of tropical SSTs remained limited in most models (e.g., Pohlmann et al. 2004; Branstator and Teng 2010; Boer 2011; Yang et al. 2013). This lack of predictability for tropical SSTs is consistent with the fact that current GCMs tend to simulate weaker than observed tropical SST anomalies associated with the AMV (e.g., Zhang and Wang 2013). Recently, Clement et al. (2015) argued that the internal component of the AMV observed during the twentieth century, and especially over the tropical region, is driven not by AMOC fluctuations but instead by chaotic atmospheric forcing. In contrast, our study shows that the North Atlantic extratropical warming tends to propagate to the tropical North Atlantic through an atmospheric circulation response indicating an extratropical origin for some of the tropical anomalies (cf. Figs. 6e,f, 7e,f, and S6). We find that this atmospheric response is too weak to lead to a tropical SST anomaly with a magnitude comparable to that of observed AMV. However, this could result from a poor simulation of clouds and of their associated feedbacks over the eastern tropical Atlantic in current GCMs, including underestimated dust–SST–rainfall feedbacks. The studies of Martin et al. (2014) and Yuan et al. (2016) indicate that these processes play a key role in extending SST anomalies from the extratropical region to the tropics via atmospheric feedbacks. Without a GCM correctly representing such processes, it appears impossible to reach a conclusion on the level of predictability of tropical SST variability of the real

world. Our study hence highlights the strong need for better understanding the drivers—both internal and external—of the tropical Atlantic decadal variability.

In the present study, we used the observed AMV, rather than the simulated one, to explore its climate impacts through GCMs. We made this choice to minimize the impact of potential model AMV biases (e.g., Zhang and Wang 2013). However, the simulated impacts analyzed in this study can still be affected by the GCM mean biases (e.g., Richter et al. 2014), which can lead to imperfect teleconnections and spurious ocean–atmosphere feedbacks as discussed by Newman et al. (2016) for the North Pacific. Further analyses need to be done to explore the effects of GCMs' mean biases on the representation of the observed AMV climate impacts. Moreover, our experimental design was designed to focus on the global influence of the AMV, but it did not allow accounting for possible feedbacks of other basins on the Atlantic SSTs, like the influence of the IPO on the AMV itself. Such feedbacks are important and should be investigated in future works. Another neglected aspect of our study concerns the possible nonlinearities of the AMV impacts. We primarily focused here on the linear climate response to the AMV by investigating the differences between the AMV+ and AMV– simulations. Another perspective of this work could be to investigate whether the AMV impacts documented in this article could change in a warmer world as suggested by Jia et al. (2016).

We acknowledge that our estimate of the internally driven component of the observed AMV is likely subject to errors resulting from limited observational data and to misrepresentations of the externally forced climate response by models (e.g., Wunderlich and Mitchell 2016; Lehner et al. 2016). Other methods have been proposed to remove the influence of external variability (e.g., by removing the linear trend of the North Atlantic mean SST; e.g., Knight et al. 2005) or by subtracting the global mean SST from the North Atlantic mean SST (e.g., Trenberth and Shea 2006). But, as discussed by Mann et al. (2014), the former method may overestimate the amplitude of the internal part of the observed AMV and misrepresent its phasing, while the latter method does not take into account the regional dependence of the externally forced response of the North Atlantic SSTs, which may result in an erroneous estimation of the AMV impacts in the experiments we consider here. More sophisticated methods based on observations have been recently proposed to remove the externally forced signal of the North Atlantic SST, such as a linear inverse model (e.g., Marini and Frankignoul 2014) or scaling methods (e.g., Frankcombe et al. 2015). To test the robustness of our results, it would then be interesting to

investigate how the different estimations of the internal component of the observed AMV impact our findings.

The main caveat of our experimental protocol comes from our choice to keep a time- and space-invariant restoring time scale. By so doing, the extratropical North Atlantic SSTs are less constrained than the tropical ones because of the spatial variations of the mixed layer depth (Figs. 15a,b). It is thus very likely that the extratropical AMV forcing in our experiments is underestimated relative to the tropical forcing. This may explain the weak atmospheric response over the NAE region in our experiments by comparison to the findings of Zhang and Delworth (2007), Peings and Magnusdottir (2015), and Davini et al. (2015), which used an atmospheric model either forced by SST or coupled to a mixed layer ocean. Nevertheless, it is also possible that their idealized configuration leads to an unrealistically strong forcing of the ocean on the atmosphere, especially in the extratropics, because of the underestimation of the heat flux damping over the ocean (e.g., Barsugli and Battisti 1998; Sutton and Matthieu 2002). To give a better estimation of the extratropical AMV forcing on the atmosphere, it would be interesting to perform similar experiments to those proposed in our study but using a restoring coefficient proportional to the mixed layer depth (e.g., Ortega et al. 2017).

In this study, we used the same experimental setup with CM2.1 and CESM1, and we found different NAE atmospheric responses, suggesting that uncertainties of the response to the AMV forcing over this region come also from different model sensitivities. These discrepancies could be due to different atmospheric resolutions or they could be linked to different representations of the stratosphere in the two models—the latter argued by Omrani et al. (2014). However, the studies of Peings and Magnusdottir (2015) and Davini et al. (2015) show that the stratosphere is not a prerequisite to simulate a NAO-like response to an AMV forcing. The response could also be sensitive to the model's mean state, but to test this hypothesis we would need further sensitivity experiments. We note that such different model sensitivities to an AMV forcing have already been found in the multimodel study of Hodson et al. (2010).

The general impacts and mechanisms described in the present study are based on two climate models that show quite similar results. This gives confidence on the robustness of our conclusions about the AMV impacts. However, conducting such experiments within a multimodel framework using other coupled climate models will be highly beneficial to strengthen our conclusions. This will be done as part of the CMIP6 Decadal Climate Prediction Project (DCPP), which calls for coordinated

experiments following a protocol similar to the one proposed in this study (Boer et al. 2016).

Acknowledgments. We thank Mingfang Ting for providing the AMV Index used in this study; Andrew Wittenberg, Xiaosong Yang, and Liping Zhang for helpful comments on an earlier version of the manuscript; Seth Underwood, Lakshmi Krishnamurthy, and Fanrong Zeng for technical help with the model runs; and anonymous reviewers who contributed to improve the quality of the manuscript through their constructive and helpful comments. The analysis and plots of this paper were performed with the NCAR Command Language (version 6.2.0; 2014), Boulder, Colorado (UCAR/NCAR/CISL/VETS; <http://dx.doi.org/10.5065/D6WD3XH5>). The CESM is supported by the NSF and the U.S. Department of Energy. This work is supported by the NSF under the Collaborative Research EaSM2 Grant OCE-1243015 to NCAR and by the NOAA Climate Program Office under the Climate Variability and Predictability Program Grant NA13OAR4310138 to NCAR and GFDL.

APPENDIX

SST Restoring

The SST restoring is performed using a restoring time scale τ_r of 5 days over a length scale of 10 m, which coincides with the thickness of the ocean models' top layer. This restoring is done through the addition of heat fluxes that act as a Newtonian damping term on the prognostic SST, proportional to its departures from the SST targeted value. The restoring coefficient value has been chosen to be small enough to allow realistic high-frequency ocean-atmosphere feedbacks to occur (Deser and Timlin 1997) but large enough to maintain the forcing we want to impose. No restoring is performed under the models' ice-covered regions. To keep the experimental protocol as simple as possible τ_r is kept constant in space and time. We note that this may lead to a weak restoring over regions with deep mixed layers (e.g., in the North Atlantic Subpolar Gyre during winter). In addition, the AMV pattern to which the SSTs are restored to is the same for all months. This does not account for the observed seasonal variations of the AMV pattern (see, e.g., Fig. 8 of Ting et al. 2014).

REFERENCES

- Barnston, A. G., and R. E. Livezey, 1987: Classification, seasonality and persistence of low-frequency atmospheric circulation patterns. *Mon. Wea. Rev.*, **115**, 1083–1126, doi:10.1175/1520-0493(1987)115<1083:CSAPOL>2.0.CO;2.

- Barsugli, J. J., and D. S. Battisti, 1998: The basic effects of atmosphere–ocean thermal coupling on midlatitude variability. *J. Atmos. Sci.*, **55**, 477–493, doi:10.1175/1520-0469(1998)055<0477:TBEAO>2.0.CO;2.
- Boer, G. J., 2011: Decadal potential predictability of twenty-first century climate. *Climate Dyn.*, **36**, 1119–1133, doi:10.1007/s00382-010-0747-9.
- , and Coauthors, 2016: The Decadal Climate Prediction Project (DCPP) contribution to CMIP6. *Geosci. Model Dev.*, **9**, 3751–3777, doi:10.5194/gmd-2016-78.
- Booth, B. B. B., N. J. Dunstone, P. R. Halloran, T. Andrews, and N. Bellouin, 2012: Aerosols implicated as a prime driver of twentieth-century North Atlantic climate variability. *Nature*, **484**, 228–232, doi:10.1038/nature10946.
- Branstator, G., and H. Teng, 2010: Two limits of initial-value decadal predictability in a CGCM. *J. Climate*, **23**, 6292–6311, doi:10.1175/2010JCLI3678.1.
- Chang, C. Y., J. C. H. Chiang, M. F. Wehner, A. R. Friedman, and R. Ruedy, 2011: Sulfate aerosol control of tropical Atlantic climate over the twentieth century. *J. Climate*, **24**, 2540–2555, doi:10.1175/2010JCLI4065.1.
- Chikamoto, Y., and Coauthors, 2012: Predictability of a stepwise shift in Pacific climate during the late 1990s in hindcast experiments using MIROC. *J. Meteor. Soc. Japan*, **90A**, 1–21, doi:10.2151/jmsj.2012-A01.
- , and Coauthors, 2015: Skillful multi-year predictions of tropical trans-basin climate variability. *Nat. Commun.*, **6**, 6869, doi:10.1038/ncomms7869.
- Chylek, P., M. K. Dubey, G. Lesins, J. Li, and N. Hengartner, 2014: Imprint of the Atlantic multi-decadal oscillation and Pacific decadal oscillation on southwestern US climate: Past, present, and future. *Climate Dyn.*, **43**, 119–129, doi:10.1007/s00382-013-1933-3.
- Clement, A., K. Bellomo, L. N. Murphy, M. A. Cane, T. Mauritsen, G. Radel, and B. Stevens, 2015: The Atlantic multidecadal oscillation without a role for ocean circulation. *Science*, **350**, 320–324, doi:10.1126/science.aab3980.
- Davini, P., J. Von Hardenberg, and S. Corti, 2015: Tropical origin for the impacts of the Atlantic multidecadal variability on the Euro-Atlantic climate. *Environ. Res. Lett.*, **10**, 094010, doi:10.1088/1748-9326/10/9/094010.
- Delworth, T. L., and Coauthors, 2006: GFDL's CM2 global coupled climate models. Part I: Formulation and simulation characteristics. *J. Climate*, **19**, 643–674, doi:10.1175/JCLI3629.1.
- Deser, C., and M. S. Timlin, 1997: Atmosphere–ocean interaction on weekly timescales in the North Atlantic and Pacific. *J. Climate*, **10**, 393–408, doi:10.1175/1520-0442(1997)010<0393:AOIOWT>2.0.CO;2.
- Dong, B., and R. T. Sutton, 2002: Adjustment of the coupled ocean–atmosphere system to a sudden change in the thermohaline circulation. *Geophys. Res. Lett.*, **29**, 1728, doi:10.1029/2002GL015229.
- , and —, 2007: Enhancement of ENSO variability by a weakened Atlantic thermohaline circulation in a coupled GCM. *J. Climate*, **20**, 4920–4939, doi:10.1175/JCLI4284.1.
- , —, and A. A. Scaife, 2006: Multidecadal modulation of El Niño–Southern Oscillation (ENSO) variance by Atlantic Ocean sea surface temperatures. *Geophys. Res. Lett.*, **33**, L08705, doi:10.1029/2006GL025766.
- Dunstone, N. J., D. M. Smith, and R. Eade, 2011: Multi-year predictability of the tropical Atlantic atmosphere driven by the high latitude North Atlantic Ocean. *Geophys. Res. Lett.*, **38**, L14701, doi:10.1029/2011GL047949.
- Ebbesmeyer, C. C., D. R. Cayan, D. R. McLain, F. H. Nichols, D. H. Peterson, and K. T. Redmond, 1991: 1976 step in the Pacific climate: Forty environmental changes between 1968–1975 and 1977–1984. *Proc. Seventh Annual Pacific Climate Workshop, April 1990*, Pacific Grove, CA, California Department of Water Resources, 115–126.
- Enfield, D. B., A. M. Mestas-Núñez, and P. J. Trimble, 2001: The Atlantic multidecadal oscillation and its relation to rainfall and river flows in the continental U.S. *Geophys. Res. Lett.*, **28**, 2077, doi:10.1029/2000GL012745.
- Folland, C. K., W. Colman, D. P. Rowell, and M. K. Davey, 2001: Predictability of northeast Brazil rainfall and real-time forecast skill, 1987–98. *J. Climate*, **14**, 1937–1958, doi:10.1175/1520-0442(2001)014<1937:PONBRA>2.0.CO;2.
- Frankcombe, L. M., A. von der Heydt, and H. A. Dijkstra, 2010: North Atlantic multidecadal climate variability: An investigation of dominant time scales and processes. *J. Climate*, **23**, 3626–3638, doi:10.1175/2010JCLI3471.1.
- , M. H. England, M. E. Mann, and B. A. Steinman, 2015: Separating internal variability from the externally forced climate response. *J. Climate*, **28**, 8184–8202, doi:10.1175/JCLI-D-15-0069.1.
- Gastineau, G., and C. Frankignoul, 2012: Cold-season atmospheric response to the natural variability of the Atlantic meridional overturning circulation. *Climate Dyn.*, **39**, 37–57, doi:10.1007/s00382-011-1109-y.
- , and —, 2015: Influence of the North Atlantic SST variability on the atmospheric circulation during the twentieth century. *J. Climate*, **28**, 1396–1416, doi:10.1175/JCLI-D-14-00424.1.
- Gill, A. E., 1980: Some simple solutions for heat-induced tropical circulation. *Quart. J. Roy. Meteor. Soc.*, **106**, 447–462, doi:10.1002/qj.49710644905.
- Goldenberg, S. B., C. W. Landsea, A. M. Mestas-Núñez, and W. M. Gray, 2001: The recent increase in Atlantic hurricane activity: Causes and implications. *Science*, **293**, 474–479, doi:10.1126/science.1060040.
- Gray, S. T., L. J. Graumlich, J. L. Betancourt, and G. T. Pederson, 2004: A tree-ring based reconstruction of the Atlantic multidecadal oscillation since 1567 A.D. *Geophys. Res. Lett.*, **31**, 2–5, doi:10.1029/2004GL019932.
- Häkkinen, S., P. B. Rhines, and D. L. Worthen, 2011: Atmospheric blocking and Atlantic multi-decadal ocean variability. *Science*, **334**, 655–660, doi:10.1126/science.1205683.
- Ham, Y.-G., and J.-S. Kug, 2015: Role of north tropical Atlantic SST on the ENSO simulated using CMIP3 and CMIP5 models. *Climate Dyn.*, **45**, 3103–3117, doi:10.1007/s00382-015-2527-z.
- Hare, S. R., and N. J. Mantua, 2000: Empirical evidence for North Pacific regime shifts in 1977 and 1989. *Prog. Oceanogr.*, **47**, 103–145, doi:10.1016/S0079-6611(00)00033-1.
- Hawkins, E., R. S. Smith, J. M. Gregory, and D. A. Stainforth, 2015: Irreducible uncertainty in near-term climate projections. *Climate Dyn.*, **46**, 3807–3819, doi:10.1007/s00382-015-2806-8.
- Held, I. M., and M. J. Suarez, 1994: A proposal for the intercomparison of the dynamical cores of atmospheric general circulation models. *Bull. Amer. Meteor. Soc.*, **75**, 1825–1830, doi:10.1175/1520-0477(1994)075<1825:APFTIO>2.0.CO;2.
- Hodson, D. L. R., R. T. Sutton, C. Cassou, N. Keenlyside, Y. Okumura, and T. Zhou, 2010: Climate impacts of recent multidecadal changes in Atlantic Ocean sea surface temperature: A multimodel comparison. *Climate Dyn.*, **34**, 1041–1058, doi:10.1007/s00382-009-0571-2.

- Horel, J., and J. Wallace, 1981: Planetary-scale atmospheric phenomena associated with the Southern Oscillation. *Mon. Wea. Rev.*, **109**, 813–829, doi:10.1175/1520-0493(1981)109<0813:PSAPAW>2.0.CO;2.
- Jia, F., L. Wu, B. Gan, and W. Cai, 2016: Global warming attenuates the tropical Atlantic-Pacific teleconnection. *Sci. Rep.*, **6**, 20078, doi:10.1038/srep20078.
- Kay, J. E., and Coauthors, 2015: The Community Earth System Model (CESM) large ensemble project: A community resource for studying climate change in the presence of internal climate variability. *Bull. Amer. Meteor. Soc.*, **96**, 1333–1349, doi:10.1175/BAMS-D-13-00255.1.
- Kerr, R., 2000: A North Atlantic climate pacemaker for the centuries. *Science*, **288**, 1984–1985, doi:10.1126/science.288.5473.1984.
- Knight, J. R., R. J. Allan, C. K. Folland, M. Vellinga, and M. E. Mann, 2005: A signature of persistent natural thermohaline circulation cycles in observed climate. *Geophys. Res. Lett.*, **32**, L20708, doi:10.1029/2005GL024233.
- Knudsen, M. F., M.-S. Seidenkrantz, B. H. Jacobsen, and A. Kuijpers, 2011: Tracking the Atlantic multidecadal oscillation through the last 8,000 years. *Nat. Commun.*, **2**, 178, doi:10.1038/ncomms1186.
- Kociuba, G., and S. B. Power, 2015: Inability of CMIP5 models to simulate recent strengthening of the Walker circulation: Implications for projections. *J. Climate*, **28**, 20–35, doi:10.1175/JCLI-D-13-00752.1.
- Krishnamurthy, L., and V. Krishnamurthy, 2015: Teleconnections of Indian monsoon rainfall with AMO and Atlantic tripole. *Climate Dyn.*, **46**, 2269–2285, doi:10.1007/s00382-015-2701-3.
- Kucharski, F., I. S. Kang, R. Farneti, and L. Feudale, 2011: Tropical Pacific response to 20th century Atlantic warming. *Geophys. Res. Lett.*, **38**, L03702, doi:10.1029/2010GL046248.
- , and Coauthors, 2015: Atlantic forcing of Pacific decadal variability. *Climate Dyn.*, **46**, 2337–2351, doi:10.1007/s00382-015-2705-z.
- Kushnir, Y., 1994: Interdecadal variations in North Atlantic sea surface temperature and associated atmospheric conditions. *J. Climate*, **7**, 141–157, doi:10.1175/1520-0442(1994)007<0141:IVINAS>2.0.CO;2.
- , R. Seager, M. Ting, N. Naik, and J. Nakamura, 2010: Mechanisms of tropical Atlantic SST influence on North American precipitation variability. *J. Climate*, **23**, 5610–5628, doi:10.1175/2010JCLI3172.1.
- Lee, S.-K., C. Wang, and B. E. Mapes, 2009: A simple atmospheric model of the local and teleconnection responses to tropical heating anomalies. *J. Climate*, **22**, 272–284, doi:10.1175/2008JCLI2303.1.
- Lehner, F., A. P. Schurer, G. C. Hegerl, C. Deser, and T. L. Fröhlicher, 2016: The importance of ENSO phase during volcanic eruptions for detection and attribution. *Geophys. Res. Lett.*, **43**, 2851–2858, doi:10.1002/2016GL067935.
- Li, X., S.-P. Xie, S. T. Gille, and C. Yoo, 2015: Atlantic-induced pan-tropical climate change over the past three decades. *Nat. Climate Change*, **6**, 275–279, doi:10.1038/nclimate2840.
- Mann, M. E., B. A. Steinman, and S. K. Miller, 2014: On forced temperature changes, internal variability, and the AMO. *Geophys. Res. Lett.*, **41**, 3211–3219, doi:10.1002/2014GL059233.
- Mantua, N. J., S. R. Hare, Y. Zhang, J. M. Wallace, and R. C. Francis, 1997: A Pacific interdecadal climate oscillation with impacts on salmon production. *Bull. Amer. Meteor. Soc.*, **78**, 1069–1079, doi:10.1175/1520-0477(1997)078<1069:APICOW>2.0.CO;2.
- Marini, C., and C. Frankignoul, 2014: An attempt to deconstruct the Atlantic multidecadal oscillation. *Climate Dyn.*, **43**, 607–625, doi:10.1007/s00382-013-1852-3.
- Martin, E. R., and C. Thorncroft, 2014: The impact of the AMO on the West African monsoon annual cycle. *Quart. J. Roy. Meteor. Soc.*, **140**, 31–46, doi:10.1002/qj.2107.
- , —, and B. B. Booth, 2014: The multidecadal Atlantic SST–Sahel rainfall teleconnection in CMIP5 simulations. *J. Climate*, **27**, 784–806, doi:10.1175/JCLI-D-13-00242.1.
- Martín-Rey, M., B. Rodríguez-Fonseca, I. Polo, and F. Kucharski, 2014: On the Atlantic–Pacific Niños connection: A multidecadal modulated mode. *Climate Dyn.*, **43**, 3163–3178, doi:10.1007/s00382-014-2305-3.
- McCabe, G. J., M. A. Palecki, and J. L. Betancourt, 2004: Pacific and Atlantic Ocean influences on multidecadal drought frequency in the United States. *Proc. Natl. Acad. Sci. USA*, **101**, 4136–4141, doi:10.1073/pnas.0306738101.
- McGregor, S., A. Timmermann, M. F. Stuecker, M. H. England, M. Merrifield, F.-F. Jin, and Y. Chikamoto, 2014: Recent Walker circulation strengthening and Pacific cooling amplified by Atlantic warming. *Nat. Climate Change*, **4**, 888–892, doi:10.1038/nclimate2330.
- Medhaug, I., and T. Furevik, 2011: North Atlantic 20th century multidecadal variability in coupled climate models: Sea surface temperature and ocean overturning circulation. *Ocean Sci.*, **8**, 389–404, doi:10.5194/os-7-389-2011.
- Minobe, S., 1997: A 50–70 year climatic oscillation over the North Pacific and North America. *Geophys. Res. Lett.*, **24**, 683–686, doi:10.1029/97GL00504.
- , 1999: Resonance in bidecadal and pentadecadal climate oscillations over the North Pacific: Role in climatic regime shifts. *Geophys. Res. Lett.*, **26**, 855–858, doi:10.1029/1999GL900119.
- Mohino, E., S. Janicot, and J. Bader, 2011: Sahel rainfall and decadal to multi-decadal sea surface temperature variability. *Climate Dyn.*, **37**, 419–440, doi:10.1007/s00382-010-0867-2.
- Msadek, R., and Coauthors, 2014: Predicting a decadal shift in North Atlantic climate variability using the GFDL forecast system. *J. Climate*, **27**, 6472–6496, doi:10.1175/JCLI-D-13-00476.1.
- Newman, M., and Coauthors, 2016: The Pacific decadal oscillation, revisited. *J. Climate*, **29**, 4399–4427, doi:10.1175/JCLI-D-15-0508.1.
- Okumura, Y. M., C. Deser, A. Hu, A. Timmermann, and S.-P. Xie, 2009: North Pacific climate response to freshwater forcing in the subarctic North Atlantic: Oceanic and atmospheric pathways. *J. Climate*, **22**, 1424–1445, doi:10.1175/2008JCLI2511.1.
- Omrani, N. E., N. S. Keenlyside, J. Bader, and E. Manzini, 2014: Stratosphere key for wintertime atmospheric response to warm Atlantic decadal conditions. *Climate Dyn.*, **42**, 649–663, doi:10.1007/s00382-013-1860-3.
- Ortega, P., E. Guilyardi, D. Swingedouw, J. Mignot, and S. Nguyen, 2017: Reconstructing extreme AMOC events through nudging of the ocean surface: A perfect model approach. *Climate Dyn.*, doi:10.1007/s00382-017-3521-4, in press.
- Otterå, O. H., M. Bentsen, H. Drange, and L. Suo, 2010: External forcing as a metronome for Atlantic multidecadal variability. *Nat. Geosci.*, **3**, 688–694, doi:10.1038/ngeo955.
- Overland, J., S. Rodionov, S. Minobe, and N. Bond, 2008: North Pacific regime shifts: Definitions, issues and recent transitions. *Prog. Oceanogr.*, **77**, 92–102, doi:10.1016/j.pocean.2008.03.016.
- Peings, Y., and G. Magnusdottir, 2014: Forcing of the wintertime atmospheric circulation by the multidecadal fluctuations of the North Atlantic Ocean. *Environ. Res. Lett.*, **9**, 034018, doi:10.1088/1748-9326/9/3/034018.
- , and —, 2015: Wintertime atmospheric response to Atlantic multidecadal variability: Dependence on stratospheric representation and ocean–atmosphere coupling. *Climate Dyn.*, **47**, 1029–1047, doi:10.1007/s00382-015-2887-4.

- Pohlmann, H., M. Botzet, M. Latif, A. Roesch, M. Wild, and P. Tschuck, 2004: Estimating the decadal predictability of a coupled AOGCM. *J. Climate*, **17**, 4463–4472, doi:10.1175/3209.1.
- Polo, I., M. Martín-Rey, B. Rodríguez-Fonseca, F. Kucharski, and C. R. Mechoso, 2015: Processes in the Pacific La Niña onset triggered by the Atlantic Niño. *Climate Dyn.*, **44**, 115–131, doi:10.1007/s00382-014-2354-7.
- Power, S., T. Casey, C. Folland, A. Colman, and V. Mehta, 1999: Inter-decadal modulation of the impact of ENSO on Australia. *Climate Dyn.*, **15**, 319–324, doi:10.1007/s003820050284.
- Richter, I., S. P. Xie, S. K. Behera, T. Doi, and Y. Masumoto, 2014: Equatorial Atlantic variability and its relation to mean state biases in CMIP5. *Climate Dyn.*, **42**, 171–188, doi:10.1007/s00382-012-1624-5.
- Robson, J., R. Sutton, K. Lohmann, D. Smith, and M. D. Palmer, 2012: Causes of the rapid warming of the North Atlantic Ocean in the mid-1990s. *J. Climate*, **25**, 4116–4134, doi:10.1175/JCLI-D-11-00443.1.
- Rodríguez-Fonseca, B., I. Polo, J. García-Serrano, T. Losada, E. Mohino, C. R. Mechoso, and F. Kucharski, 2009: Are Atlantic Niños enhancing Pacific ENSO events in recent decades? *Geophys. Res. Lett.*, **36**, L20705, doi:10.1029/2009GL040048.
- Rotstajn, L. D., and U. Lohmann, 2002: Tropical rainfall trends and the indirect aerosol effect. *J. Climate*, **15**, 2103–2116, doi:10.1175/1520-0442(2002)015<2103:TRTATI>2.0.CO;2.
- Ruprich-Robert, Y., and C. Cassou, 2015: Combined influences of seasonal East Atlantic Pattern and North Atlantic Oscillation to excite Atlantic multidecadal variability in a climate model. *Climate Dyn.*, **44**, 229–253, doi:10.1007/s00382-014-2176-7.
- Schlesinger, M. E., and N. Ramankutty, 1994: An oscillation in the global climate system of period 65–70 years. *Nature*, **367**, 723–726, doi:10.1038/367723a0.
- Schubert, S., and Coauthors, 2009: A U.S. CLIVAR project to assess and compare the responses of global climate models to drought-related SST forcing patterns: Overview and results. *J. Climate*, **22**, 5251–5272, doi:10.1175/2009jcli3060.1.
- Seager, R., N. Naik, W. Baethgen, A. Robertson, Y. Kushnir, J. Nakamura, and S. Jurburg, 2010a: Tropical oceanic causes of interannual to multidecadal precipitation variability in southeast South America over the past century. *J. Climate*, **23**, 5517–5539, doi:10.1175/2010JCLI3578.1.
- , —, M. Ting, M. A. Cane, N. Harnik, and Y. Kushnir, 2010b: Adjustment of the atmospheric circulation to tropical Pacific SST anomalies: Variability of transient eddy propagation in the Pacific–North America sector. *Quart. J. Roy. Meteor. Soc.*, **136**, 277–296, doi:10.1002/qj.588.
- Smirnov, D., and D. J. Vimont, 2012: Extratropical forcing of tropical Atlantic variability during boreal summer and fall. *J. Climate*, **25**, 2056–2076, doi:10.1175/JCLI-D-11-00104.1.
- Smith, T. M., R. W. Reynolds, T. C. Peterson, and J. Lawrimore, 2008: Improvements to NOAA's historical merged land-ocean surface temperature analysis (1880–2006). *J. Climate*, **21**, 2283–2296, doi:10.1175/2007JCLI2100.1.
- Sutton, R., and P.-P. Mathieu, 2002: Response of the atmosphere–ocean mixed-layer system to anomalous ocean heat-flux convergence. *Quart. J. Roy. Meteor. Soc.*, **128**, 1259–1275, doi:10.1256/003590002320373283.
- , and D. L. R. Hodson, 2005: North Atlantic forcing of North American and European summer climate. *Science*, **309**, 115–118, doi:10.1126/science.1109496.
- , and —, 2007: Climate response to basin-scale warming and cooling of the North Atlantic Ocean. *J. Climate*, **20**, 891–907, doi:10.1175/JCLI4038.1.
- , and B. Dong, 2012: Atlantic Ocean influence on a shift in European climate in the 1990s. *Nat. Geosci.*, **5**, 788–792, doi:10.1038/ngeo1595.
- Swingedouw, D., J. Mignot, S. Labetoulle, E. Guilyardi, and G. Madec, 2013: Initialization and predictability of the AMOC over the last 50 years in a climate model. *Climate Dyn.*, **40**, 2381–2399, doi:10.1007/s00382-012-1516-8.
- Tang, Y., D. Chen, D. Yang, and T. Li, 2013: Methods of estimating uncertainty of climate prediction and climate change projection. *Climate Change: Realities, Impacts over Ice Cap, Sea Level and Risks*, B. R. Singh, Ed., InTech, 397–420, doi:10.5772/54810.
- Terray, L., 2012: Evidence for multiple drivers of North Atlantic multi-decadal climate variability. *Geophys. Res. Lett.*, **39**, L19712, doi:10.1029/2012GL053046.
- Timmermann, A., and Coauthors, 2007: The influence of a weakening of the Atlantic meridional overturning circulation on ENSO. *J. Climate*, **20**, 4899–4919, doi:10.1175/JCLI4283.1.
- Ting, M., Y. Kushnir, R. Seager, and C. Li, 2009: Forced and internal twentieth-century SST trends in the North Atlantic. *J. Climate*, **22**, 1469–1481, doi:10.1175/2008JCLI2561.1.
- , —, —, and —, 2011: Robust features of Atlantic multidecadal variability and its climate impacts. *Geophys. Res. Lett.*, **38**, L17705, doi:10.1029/2011GL048712.
- , —, and C. Li, 2014: North Atlantic multidecadal SST oscillation: External forcing versus internal variability. *J. Mar. Syst.*, **133**, 27–38, doi:10.1016/j.jmarsys.2013.07.006.
- Trenberth, K. E., and D. J. Shea, 2006: Atlantic hurricanes and natural variability in 2005. *Geophys. Res. Lett.*, **33**, L12704, doi:10.1029/2006GL026894.
- , G. W. Branstator, D. Karoly, A. Kumar, N. C. Lau, and C. Ropelewski, 1998: Progress during TOGA in understanding and modeling global teleconnections associated with tropical sea surface temperatures. *J. Geophys. Res.*, **103**, 14 291–14 324, doi:10.1029/97jc01444.
- Vimont, D. J., and J. P. Kossin, 2007: The Atlantic meridional mode and hurricane activity. *Geophys. Res. Lett.*, **34**, L07709, doi:10.1029/2007GL029683.
- Wallace, J. M., and D. S. Gutzler, 1981: Teleconnections in the geopotential height field during the Northern Hemisphere winter. *Mon. Wea. Rev.*, **109**, 784–812, doi:10.1175/1520-0493(1981)109<0784:TITGHF>2.0.CO;2.
- Wang, C., S.-K. Lee, and D. B. Enfield, 2008: Climate response to anomalously large and small Atlantic warm pools during the summer. *J. Climate*, **21**, 2437–2450, doi:10.1175/2007JCLI2029.1.
- , S. Dong, A. T. Evan, G. R. Foltz, and S.-K. Lee, 2012: Multidecadal covariability of North Atlantic sea surface temperature, African dust, Sahel rainfall, and Atlantic hurricanes. *J. Climate*, **25**, 5404–5415, doi:10.1175/JCLI-D-11-00413.1.
- Wittenberg, A. T., A. Rosati, N. C. Lau, and J. J. Ploshay, 2006: GFDL's CM2 global coupled climate models. Part III: Tropical Pacific climate and ENSO. *J. Climate*, **19**, 698–722, doi:10.1175/JCLI3631.1.
- Wu, L., F. He, and Z. Liu, 2005: Coupled ocean-atmosphere response to north tropical Atlantic SST: Tropical Atlantic dipole and ENSO. *Geophys. Res. Lett.*, **32**, L21712, doi:10.1029/2005GL024222.

- Wunderlich, F., and D. M. Mitchell, 2016: Uncertainty and detectability of climate surface response to large volcanic eruptions. *Atmos. Chem. Phys.*, **17**, 485–499, doi:10.5194/acp-2016-173.
- Yamamoto, A., and J. B. Palter, 2016: The absence of an Atlantic imprint on the multidecadal variability of wintertime European temperature. *Nat. Commun.*, **7**, 10930, doi:10.1038/ncomms10930.
- Yang, X., and Coauthors, 2013: A predictable AMO-like pattern in the GFDL fully coupled ensemble initialization and decadal forecasting system. *J. Climate*, **26**, 650–661, doi:10.1175/JCLI-D-12-00231.1.
- Yeager, S., A. Karspeck, G. Danabasoglu, J. Tribbia, and H. Teng, 2012: A decadal prediction case study: Late twentieth-century North Atlantic Ocean heat content. *J. Climate*, **25**, 5173–5189, doi:10.1175/JCLI-D-11-00595.1.
- Yuan, T., L. Oreopoulos, M. Zelinka, H. Yu, J. R. Norris, M. Chin, S. Platnick, and K. Meyer, 2016: Positive low cloud and dust feedbacks amplify tropical North Atlantic Multidecadal Oscillation. *Geophys Res Lett.*, **43**, 1349–1356, doi:10.1002/2016GL067679.
- Zanchettin, D., O. Bothe, H. F. Graf, N. Omrani, A. Rubino, and J. H. Jungclaus, 2016: A decadal delayed response of the tropical Pacific to Atlantic multidecadal variability. *Geophys. Res. Lett.*, **43**, 784–792, doi:10.1002/2015GL067284.
- Zhang, L., and C. Wang, 2013: Multidecadal North Atlantic sea surface temperature and Atlantic meridional overturning circulation variability in CMIP5 historical simulations. *J. Geophys. Res. Oceans*, **118**, 5772–5791, doi:10.1002/jgrc.20390.
- , and T. L. Delworth, 2015: Analysis of the characteristics and mechanisms of the Pacific decadal oscillation in a suite of coupled models from the Geophysical Fluid Dynamics Laboratory. *J. Climate*, **28**, 7678–7701, doi:10.1175/JCLI-D-14-00647.1.
- , and C. Zhao, 2015: Processes and mechanisms for the model SST biases in the North Atlantic and North Pacific: A link with the Atlantic meridional overturning circulation. *J. Adv. Model. Earth Syst.*, **7**, 739–758, doi:10.1002/2014MS000415.
- Zhang, R., 2008: Coherent surface-subsurface fingerprint of the Atlantic meridional overturning circulation. *Geophys. Res. Lett.*, **35**, L07403, doi:10.1029/2008GL033222.
- , and T. L. Delworth, 2005: Simulated tropical response to a substantial weakening of the Atlantic thermohaline circulation. *J. Climate*, **18**, 1853–1860, doi:10.1175/JCLI3460.1.
- , and —, 2006: Impact of Atlantic multidecadal oscillations on India/Sahel rainfall and Atlantic hurricanes. *Geophys. Res. Lett.*, **33**, L17712, doi:10.1029/2006GL026267.
- , and —, 2007: Impact of the Atlantic multidecadal oscillation on North Pacific climate variability. *Geophys. Res. Lett.*, **34**, L23708, doi:10.1029/2007GL031601.
- Zhang, Y., J. M. Wallace, and D. S. Battisti, 1997: ENSO-like interdecadal variability: 1900–93. *J. Climate*, **10**, 1004–1020, doi:10.1175/1520-0442(1997)010<1004:ELIV>2.0.CO;2.

Copyright of Journal of Climate is the property of American Meteorological Society and its content may not be copied or emailed to multiple sites or posted to a listserv without the copyright holder's express written permission. However, users may print, download, or email articles for individual use.